Anterior-posterior polarity signals differentially regulate regeneration-competence of the tapeworm *Hymenolepis diminuta*.

Elise McCollough Nanista[1], Landon Elizabeth Poythress[1], Isabell Reese Skipper[1], Trevor Haskins[1], Marieher Felix Cora[2] and Tania Rozario[1]*

[1]University of Georgia, Athens, GA, USA

[2]University of Puerto Rico-Cayey, PR, USA

Running title: Tapeworm regeneration-competence

* corresponding author

tania.rozario@uga.edu

500 D.W. Brooks Dr., Athens, GA 30602, USA

ORCIDS:

EMN: 0009-0002-3844-876X

LEP: 0009-0007-5836-5714

IRS: 0009-0009-1869-7292

TH: 0009-0007-1528-3807

MFC: 0009-0004-9971-0826

TR: 0000-0002-9971-5211

Keywords: regeneration, tapeworm, planaria, flatworm, Wnt signaling

Abstract

Competence to regenerate lost tissues varies widely across species. The rat tapeworm, *Hymenolepis diminuta*, undergoes continual cycles of shedding and regenerating thousands of reproductive segments to propagate the species. Despite its prowess, *H. diminuta* can only regenerate posteriorly from a singular tissue: the neck or germinative region (GR). What cells and signaling pathways restrict regeneration competence to the GR? In this study, we show that the head regulates regeneration-competence by promoting maintenance of the GR and inhibiting proglottid formation in a distance-dependent manner. Anterior-posterior (A-P) patterning within the GR provide local signals that mediate these head-dependent responses. *βcat1* is necessary for stem cell maintenance, proliferation and proglottidization. On the other hand, *sfrp* is necessary for maintaining the GR at its proper length. Our study demonstrates that the head organizes a balance of pro- and anti-regeneration signals that must be integrated together and therefore control competence to regenerate.

Summary statement

We uncover how the tapeworm head organizes pro- and anti-regeneration signals that control competence to regenerate at prolific rates.

Introduction

Regeneration occurs over a wide range of biological scales from regeneration of axons at the cellular scale to whole body regeneration in planarians and hydra (Bely and Nyberg, 2010). Tapeworms represent a fascinating case study in the field of regeneration. They descend from a monophyletic clade (Neodermata) exclusively populated by parasites within the Playhelminthes phylum (Laumer et al., 2015). As a sister group to planarians, it is tempting to assume that shared regenerative abilities have enabled tapeworms to achieve their monstrous growth potential and reproductive prowess. In the normal life cycle of many adult tapeworms, large pieces of their body are shed to disperse the developing embryos for consumption by an intermediate host. Simultaneously, the adult tapeworm continues to replenish the lost tissue in the intestine. Studies with the rat tapeworm, *Hymenolepis diminuta*, demonstrated that serially transplanting anterior pieces of tapeworms into new host intestines could greatly extend the lifespan of this parasite (Goodchild, 1958; Read, 1967). *H. diminuta* can regenerate all lost reproductive segments (proglottids) and may not inherently need to age and die. However, regeneration only occurs from one anatomical structure: the neck or germinative region (GR) (Rozario et al., 2019). *H. diminuta* regeneration is dependent on a large and heterogeneous population of adult stem cells that are distributed throughout the body and do not preferentially reside in the GR (Rozario et al., 2019). By transplanting cells from regeneration-competent and regeneration-incompetent regions into lethally irradiated tapeworm GRs, we previously demonstrated that proglottid regeneration is independent of stem cell source (Rozario et al., 2019), suggesting that signals within the GR play important roles in regulating tapeworm regeneration.

A plethora of signals likely operate in the GR and control stem cell proliferation, survival, differentiation, as well as proglottidization and competence to regenerate. What these signals are and how they operate is largely unknown. Here we show that regeneration competence is tightly linked to signals from the head. The head plays seemingly contradictory roles as it is necessary to maintain the GR but negatively regulates proliferation and proglottid regeneration. We find two genes typically associated with Wnt signaling, *sfrp and βcatenin1*, as critical mediators of each head-dependent phenotype. Our study demonstrates that for successful proglottid regeneration to occur, a balance of pro- and anti-regeneration signals must be overcome to enable GR regeneration

74 and then initiation of proglottids. *H. diminuta* provides a fascinating example of how extrinsic
75 signals can promote or restrict the ability to regenerate.

Results

H. diminuta is competent to regenerate the GR.

The basic adult body plan of *H. diminuta* includes a head (scolex), an unsegmented GR and a strobilated body made of metameric proglottids (Fig. 1A). *H. diminuta* cannot regenerate its anterior or head but can regenerate proglottids from the GR when amputated outside of the GR (Rozario et al., 2019). The GR is the only regeneration-competent tissue, but it is unclear if the GR itself can regenerate. Nuclei staining with DAPI enables a quick and easy way to observe and measure the GR, which is defined as the region between the base of the head and the first proglottid. When tapeworms are continuously grown in vitro, the GR length is typically 1 mm (Rozario et al., 2019). After acclimating worms to in vitro culture conditions for 3 days, we amputated within the GR (0.5 mm) vs. outside the GR (2 mm) and grew the anterior fragments for 15 days. In both cases, proglottids were regenerated (Fig. 1A). Regenerates that were amputated within the GR, successfully formed 1 mm long GRs 15 days post amputation (dpa) comparable to regenerates that were amputated outside of the GR (Fig. 1B). The 0.5 mm fragments first regenerated GRs within 2-4 days before new proglottids were added (Fig. 1C). Once proglottids were formed, the rate of proglottid regeneration was comparable between 0.5 mm and 2 mm fragments, at 14-15 proglottids per day (Fig. 1C). Growth curves for both regenerates were also comparable and non-linear since individual proglottids increase in length as they mature (Rozario et al., 2019). Thus, when amputated within the GR, *H. diminuta* is capable of regenerating the posterior GR and subsequently proglottids.

The GR is patterned by differentially expressed genes along the anterior-posterior (A-P) axis (Rozario et al., 2019). If *H. diminuta* can regenerate its GR, then A-P polarized patterns should be restored following amputation. We performed whole mount in situ hybridization (WISH) for three posterior-enriched transcripts: *βcatenin1* (*βcat1*), *frizzled5/8* (*fzd5/8*), and *tumor necrosis factor receptor-16* (*tnfr16*) and one anterior-enriched transcript: *secreted frizzled related protein* (*sfrp*) (Fig. 1D; uncut). At 0 dpa, all markers were reduced or lost but normal A-P polarized patterns in successful regenerates were restored by at least 10 dpa demonstrating normal GR patterning (Fig. 1D). These data indicate that *H. diminuta* can successfully regenerate its GR and reestablish AP patterning within 10 days.

GR regeneration fails after serial amputation.

Regeneration of proglottids is a stem cell-driven process and can occur after multiple rounds of serial amputation (Goodchild, 1958; Read, 1967; Rozario et al., 2019). Is GR regeneration similarly robust? We amputated worms within the GR and allowed them to regenerate for 18 days before re-amputating within the GR (Fig. 2A). Subsets of each group were fixed and analyzed to capture the variation and reproducibility of the amputations performed. Amputations were targeted at the half-way point or ~0.5 mm in worms that were briefly immobilized in cold media. We find that tissues extend slightly after heat-killing and fixation resulting in slightly longer 0 dpa fragments: 0.63±0.07 mm and 0.61±0.16 mm after each amputation (Fig. 2B). The percentage of GR length retained calculated over the mean GR length of uncut worms was close to the target range of 50% and was not statistically significant between the two amputations (48±9% after cut 1 and 56±11% after cut 2) (Fig. 2C). Despite making comparable cuts at each timepoint, marked differences in regeneration were observed after the second amputation within the GR (Fig. 2D-F). Successful regenerates were almost always produced after cut 1 but ranged wildly between 10-100% regeneration after cut 2 (Fig. 2E). When worms did regenerate after cut 2, they were significantly shorter (Fig. 2D) and produced fewer proglottids (Fig. 2F). The additional challenge of serial amputation revealed that GR regeneration does fail under certain conditions.

Signals from the head regulate proglottid regeneration and maintenance of the GR.

When amputated within the GR, the wound site was closer to the head. Could the head be exerting a negative effect on regeneration? Following head amputation, regenerates exhibited increased growth and proglottid regeneration (Fig. 3A) indicating that signals from the head do inhibit growth. Using thymidine analog F-*ara*-EdU incorporation to quantify the density of proliferating cells in the GR, we found that head amputation resulted in increased proliferation, which can explain the increased growth (Fig. 3B). In uncut worms, proliferation density in the GR increases with distance from the head (Fig. 3C) further supporting our conclusion that the head provides anti-proliferation signals. Upon head amputation and in vitro culture for 3 days, the increasing proliferation density along the GR A-P axis was no longer significant (Fig. 3D). However, the curves did not fully flatten and the pattern of decreased proliferation toward the most anterior was still detectable. This suggests that while signals from the head do regulate proliferation in the GR, the effects are mediated by factors resident within the GR as well.

Many regenerating animals respond by increasing proliferation at the wound site. Is this true in *H. diminuta*? Following amputation in the GR, we quantified proliferation at both anterior- and posterior-facing wounds and found increased proliferation (Fig. S1). However, the local increase in proliferation was equivalent regardless of head presence (Fig. S1) indicating that amputation itself does not explain the increased proliferation in -head regenerates. This implies that the head does indeed negatively regulate proliferation.

In addition to proliferation within the GR, maintenance of GR tissue must also be preserved as regeneration cannot occur without it. Previous results have shown that GR maintenance depends on the head; after head amputation, the GR is eventually lost, the regenerates become fully proglottidized and cannot continue adding proglottids (Rozario et al., 2019). To further characterize how the head affects proglottid regeneration and GR maintenance, four amputation schemes were compared: + head, ½ head, -head, and -0.5 mm anterior (Fig. 4A). Of these four schemes, making transverse cuts through the head was the most challenging. A sampling of ½ head fragments were fixed immediately and stained with anti-SYNAPSIN antibodies to visualize the nervous system. Though the amount of head tissue removed did vary, the brain was always retained (Fig. S2A: yellow arrowheads). After making the four different amputations at the anterior region, we tested how the four fragment types would regenerate following serial amputation. All worms were amputated posteriorly to obtain 2 mm fragments that were grown in vitro for 14 days, then re-amputated for 3 more cycles (Fig. 4A). The posteriors of regenerates were fixed and analyzed to determine the number of proglottids regenerated after every cycle. As previously reported (Rozario et al., 2019), tapeworms regenerated after serial amputation when the head was present (Fig. 4B). The ½ head regenerates consistently displayed increased proglottid regeneration compared to +head regenerates (Fig. 4B). Both +head and ½ head regenerates maintained their GRs throughout 2 months of in vitro culture. When the head was amputated completely (-head), proglottid regeneration eventually ceased though some regenerates still had GRs after the 4th amputation (Fig. 4B). However, the GR lengths in -head regenerates that were not fully proglottidized were significantly shorter (Fig. S2B) indicating that complete proglottidization was imminent. Previously, we observed rapid loss of the GR after head amputation, but anterior GR tissue was also removed in those experiments (Rozario et al., 2019). Cognizant of regional

differences along the A-P axis of the GR, we were careful to make minimal head amputations that retained as much anterior GR as possible in this study. We find that the GR persists for much longer than previously reported but does eventually recede. On the other hand, fragments in which both the head and anterior GR were removed (-0.5 mm) became fully proglottidized by the second amputation or earlier (Fig. 4B). In sum, GRs were maintained if the brain region was retained but GRs were lost when more and more anterior tissue was removed (Fig. 4C).

The number of proglottids regenerated was also dependent on amputations at the head though our analysis was complicated by GR loss in -head and -0.5mm fragments. After the first amputation, a clear dose-dependent response was detected; when more head tissue was retained, the number of proglottids decreased (Fig. S2C). This trend was maintained after serial rounds of amputation when comparing +head and ½ head regenerates where GRs were not lost (Fig. S2D). After the 4th round of amputation, the remaining head area plotted against number of proglottids for +head and ½ head regenerates revealed a negative correlation between head tissue abundance and proglottidization (Fig. 4D). We also measured the effect of head tissue abundance on proliferation within the GR using F-*ara*-EdU. A general trend of increasing proliferation with decreasing head and anterior tissue emerged though differences between +head and ½ head were not statistically significant (Fig. 4E-F). Taken together, the head effects on maintaining the GR and regulating proliferation can be separated. Signals from the brain region are necessary to maintain the GR whereas proliferation and proglottidization are regulated by head-dependent signals in a dose-dependent manner.

βcatenin1 is necessary for proglottid regeneration and stem cell maintenance.

What is the molecular basis for the head-dependent effects on tapeworm regeneration? The Wnt signaling pathway has been implicated in A-P polarity across many systems (Petersen and Reddien, 2009) and plays roles in regulating cell proliferation, survival, and differentiation (Nusse and Clevers, 2017). Multiple members of the Wnt signaling pathway were found to be either anterior-enriched or posterior-enriched after RNA sequencing along the A-P axis of the GR (Rozario et al., 2019). As βcatenin protein is a key downstream effector of Wnt signaling, we decided to examine its function further. *H. diminuta* has three *βcatenin* paralogs as do other parasitic flatworms (Montagne et al., 2019). BLASTp comparisons of putative *H. diminuta*

βcatenin paralogs with published sequences for other flatworms (*Schmidtea medditerranea*, *Schistosoma mansoni and Ecchinococcus multilocularis*) demonstrated that *Hdim-βcat1* (WMSIL1_LOCUS14475) is the rat tapeworm ortholog of *βcat1* (Table S1). *Hdim-βcat1* retains expected conserved domains including multiple armadillo repeats and the DSGxxSxxx[S/T]xxxS motif for CKI/GSK-phosphorylation necessary for targeting by the destruction complex (Montagne et al., 2019; Valenta et al., 2012) (Fig. S3A). Capacity to bind α-catenin cannot be ruled in or out at present (Fig. S3B; discussed further below). Thus *Hdim-βcat1* likely mediates Wnt signaling and may also function in cell adhesion.

Where is *Hdim-βcat1* (hereafter *βcat1*) expressed in *H. diminuta*? In 6-day-old adults, *βcat1* expression is largely absent in the head and anterior GR but progressively increases toward the posterior GR (Fig. 5A). *βcat1* is also expressed throughout the body, in transverse stripes at proglottid boundaries and within a subset of accessory reproductive structures (Fig. S4). The broad expression pattern throughout the worm indicates that *βcat1* is expressed in many tissues and is not restricted to a particular cell type. The posterior-biased pattern of *βcat1* expression was restored after successful GR regeneration (Fig. 1D) leading us to wonder if *βcat1* is necessary for proliferation and proglottidization from the GR. We performed RNAi by injecting double-stranded RNA (dsRNA) targeting *βcat1* throughout the GR. 2 mm anterior fragments were amputated and grown in vitro to assay regenerative ability. A dramatic growth defect was captured just 7 dpa/10 days post injection (dpi) (Fig. 5B). Decreased growth was evident by 3 dpa and this RNAi treatment was ultimately lethal. The proglottids formed were extremely small and impossible to quantify but there was a marked decrease in worm lengths following *βcat1* RNAi (Fig. 5C). RNAi of *βcat1* reduced transcript levels to 8.7±2.0% (Fig. 5D). As *βcat1*-dependent Wnt signaling is mediated through degradation of βCAT1 protein by the destruction complex, we investigated expression of a key destruction complex component: *axin1*. Previous work has demonstrated that tapeworm *E. multilocularis,* AXIN proteins directly interact with Emul-βCAT1 and overexpression of Emul-AXIN1 results in degradation of Emul-βCAT1 (Montagne et al., 2019). We find that after *βcat1* RNAi, *axin1* expression is markedly reduced to 18.8±11.1% of normal levels (Fig. 5D). This suggests that canonical Wnt signaling is inhibited following *βcat1* RNAi though other roles for *βcat1* cannot be ruled out.

The strong decrease in growth after *βcat1* RNAi suggests that the cycling stem cell population in the GR is likely dependent on *βcat1*. We measured proliferation in the GR and detected a dramatic decrease in dividing cells compared to controls (Fig. 5E). This suggests that the stem cell population likely cannot be maintained in the absence of *βcat1*. To visualize the stem cell population, we performed WISH for two known stem cell markers in *H. diminuta*: *minichromosome maintenance complex component-2* (*mcm2*) and *laminB receptor* (*lbr*) (Rozario et al., 2019). Both stem cell markers showed decreased expression indicating that *βcat1* is required to maintain stem cells in the GR (Fig. 5F).

GR maintenance requires *sfrp*.

Our analyses so far suggest that signals from the head set up gene expression patterns within the GR with posteriorly enriched *βcat1* playing indispensable roles in maintaining stem cells. However, it is unclear if *βcat1* regulates stem cell maintenance through Wnt signaling, cell adhesion or both. If Wnt signaling is necessary, the head may segregate Wnt inhibitors toward the anterior. Previously, RNA sequencing of A-P polarized transcripts in the GR found that *sfrp* was anterior-enriched (Rozario et al., 2019). Like other tapeworms, *H. diminuta* has one true *sfrp* family member and a second highly divergent member, *sfrp-like*, which was not investigated further in this study. Interpro (Blum et al., 2020) predicts that Hdim-SFRP retains both frizzled and netrin domains albeit with some variation (Fig. S5; discussed further below). Since SFRP can inhibit Wnt signaling (Leyns et al., 1997; Rattner et al., 1997; Wang et al., 1997), we decided to pursue its potential role in regeneration.

By WISH, *sfrp* expression is strikingly anterior-enriched. We detected *sfrp* expression sparsely within the head and strongly throughout the GR with expression tapering off posteriorly (Fig. 6A). In adult tapeworms, *sfrp* expression is largely absent from the strobilated body except at the lateral ends of proglottids (Fig. S4). Perhaps knocking down *sfrp* would result in the opposite phenotypes observed from *βcat* RNAi and would phenocopy head amputation. We injected dsRNA into the head, amputated 2 mm anterior fragments, reinjected dsRNA into the head and collected worms at 10-12 dpa (Fig. 6B). Contrary to our expectations, a modest decrease in worm lengths and proglottid regeneration were observed (Fig. 6C-D). Strikingly, we discovered that the GRs were

significantly shortened following *sfrp* RNAi (Fig. 6E-F). This is the first time GR length has been affected by RNAi of any target gene. Injecting dsRNA into the head does not preclude diffusion into the GR but the knockdown is likely to be anteriorly biased. If so, we may inadvertently miss other potential roles for *sfrp* toward the posterior GR. We injected dsRNA throughout the GR and observed the same phenotypes (Fig. S6A-D). Both injection schemes resulted in similar *sfrp* knockdown efficacy (Fig. S6E). While the levels of knockdown did vary substantially, GR length reduction was consistently observed.

Our results indicate that *sfrp* is necessary for proper GR maintenance but is unlikely to be involved in head-dependent inhibition of proliferation or proglottidization. Instead, *sfrp* likely mediates head-dependent GR maintenance. Accordingly, we observed decreased *sfrp* expression just 3 days after head amputation (Fig. 6G). This correlation supports the conclusion that the failure to maintain the GR after head amputation is mediated through anterior-enriched *sfrp* expression.

Decreased proglottid regeneration after *sfrp* RNAi does not support the hypothesis that *sfrp* functions as a Wnt inhibitor. Proliferation within the GR was not significantly changed after *sfrp* RNAi (Fig. S5D). However, the shortening of the GR would bring the posterior boundary of the GR closer to the head. Thus, *sfrp* RNAi may indirectly exacerbate the anti-proglottidization and anti-proliferation effects from the head.

Amputation distance from the head determines whether pro- or anti-regeneration signals dominate.

The mechanisms that govern the two head-dependent effects on regeneration have begun to emerge. The presence of the head is necessary for *sfrp* expression and GR maintenance. However, the presence of the head also inhibits proliferation and proglottidization, which are dependent on *βcat1*. Perhaps when the posterior wound is too close to the head, the growth inhibitory effect of the head dominates, and GR regeneration fails. This suggests that regeneration would fail more when the posterior cut is made at decreasing distance from the head. To test this, worms were allowed to regenerate after 0.5 mm amputation within the GR and then cut a second time at 4 different distances from the head. All samples were cut at ~1mm and then subsets were progressively shaved closer and closer toward the head (Fig. 7A; cuts A-D). Subsets of fragments

were fixed at 0 dpa and we verified that cut A-D progressively retained 87±5%, 64±7%, 47±9%, and 22±4% of the GR (Fig. 7B). As expected, GR and proglottid regeneration plummeted at cut B or C over three independent experiments (Fig. 7C). Surprisingly, the smallest fragments (cut D) regenerated equivalently to the longest fragments (cut A) (Fig. 7C-D and Fig. S7). Fragments from cut A and D achieved different absolute lengths at 18 dpa but the fold change in growth was comparable (Fig. 7E). Also, no significant difference is GR length was detected in regenerates from cut A or D (Fig. 7F). Thus, the inhibitory effect of the head was overcome when enough posterior GR tissue was removed. These results suggest that there are yet more signals to be uncovered that explain how regeneration is promoted and restricted in tapeworms.

While there is still much to discover, we propose the following working model (Fig. 8A). The head likely produces direct or indirect inhibitor(s) of a posterior signal that we dub factor X. Factor X may be posterior Wnts, other signaling pathways that crosstalk with Wnt signaling or Wnt-independent signals. The head promotes *sfrp* expression, which is necessary to maintain the GR. The posterior GR produces a counteracting signal that results in stable maintenance of the GR length. Factor X acts via *βcat1* to promote proglottid formation. Proglottids only form at sufficient distance from the head where high *βcat1* activity is present. Upon head amputation (Fig. 8B), *sfrp* expression is inhibited causing the posterior boundary of the GR to creep up towards the anterior. Without the head, inhibition of factor X is relieved and overstimulation of *βcat1* results in increased proglottid regeneration until the GR is fully lost.

Our experiments also demonstrated that cutting within the GR produced highly mixed results, which can now be explained by our model. Tapeworms grown in vitro are adjusting to a new environment and all tissue dimensions change with time. The various amputation schemes within the GR used throughout this paper revealed that depending on the state of signaling gradients from the head and GR, we pushed regeneration competence toward a pro- or anti-regeneration state. When cuts were made “mid” GR at an unfavorable distance from the head (Fig. 8C), inhibition of factor X dominated leading to failure to regenerate proglottids. However, when a minimal fragment was produced (Fig. 8D), perhaps the absence of factor X negates the inhibitory functions of the head. The head could promote establishment of *sfrp* and proper growth of the GR. At a sufficient distance from the head, factor X is now stimulated and can promote proglottid

323 regeneration. The exact players, direct and indirect relationships, as well as additional molecular
324 mechanisms predicted by our working model still need to be tested but the general take-home
325 holds: a balance of pro- and anti-regeneration factors operate in the GR of *H. diminuta*.

Discussion

Regenerative abilities vary widely even amongst species that are competent to regenerate. Thus, it is important to understand the factors that both promote and inhibit regeneration. The flatworm phylum offers opportunities to study variations in regenerative abilities. While the free-living planarian *S. mediterranea* can regenerate from almost any amputation fragment, regeneration in *H. diminuta* is far more limited. This study explores how a balance of activating and inhibiting signals operate in the regeneration-competent region: the GR.

We show that in addition to regenerating proglottids, *H. diminuta* can also regenerate the posterior GR following amputation. However, the challenge of serial amputation within the GR revealed that there are anti-regeneration factors that were previously unknown. By testing amputation schemes at the anterior, we revealed that the head plays at least two seemingly contradictory roles: 1) the head promotes GR maintenance and 2) the head inhibits proliferation within the GR and proglottid regeneration. Interestingly, these two roles can be separated both anatomically and through molecular regulators.

GR maintenance depends on the brain-region without which the GR will eventually be lost. Loss of the GR is gradual unless the anterior GR is also removed. The head likely acts as an organizer that relays signals within the GR. In this model, total loss of the GR will occur after anterior-enriched patterns within the GR turnover and cannot be reestablished following head amputation. One critical mediator of head-dependent GR maintenance is *sfrp*. Like head amputation, RNAi of *sfrp* results in shortened GRs. However, *sfrp* RNAi does not phenocopy the growth spurts observed after head amputation. The mechanism by which *sfrp* maintains the GR is more mysterious. While *sfrp* is primarily known as a Wnt antagonist, it has also been shown to bind and stimulate frizzled receptors, interact with other signaling pathways and modulate cell-matrix interactions by binding integrins (Bovolenta et al., 2008; Mii and Taira, 2011). There is evidence that *sfrps* can stimulate Wnt and BMP signaling in the zebrafish retina (Holly et al., 2014). In Drosophila, *sfrps* can modulate Wnt signaling in a biphasic manner: inhibiting Wnt signaling when expressed at high levels while promoting Wnt signaling when expressed at low levels (Üren et al., 2000). In *H. diminuta*, the *sfrp* RNAi phenotypes were not the opposite of the *βcat1* RNAi phenotypes as one

might predict if *sfrp* and *βcat1* were acting solely as Wnt antagonist and Wnt effector respectively. Nonetheless, it is still possible that *sfrp* is inhibiting Wnt signaling. In many flatworms, Wnt ligands are secreted from both anterior and posterior domains (Armstrong et al., 2025; Koziol et al., 2016; Reddien, 2018; Soria et al., 2020). Expression of *sfrp* throughout the GR may be required as a permissive signal to tune Wnt signaling to a moderately low level so that it can be acted upon differentially by other modulators. Alternatively, *sfrp* may be functioning independent of Wnt signaling. Future studies investigating the RNAi phenotypes of other Wnt antagonists, Wnt ligands and frizzed receptors will be necessary to determine how Wnt signaling regulates individual cell- and tissue-level behaviors at the GR that are necessary for regeneration.

A further complication is that the biochemical properties and interactors of SFRP proteins in flatworms in not well understood. Both frizzled and netrin domains are readily identifiable in flatworm SFRPs. The netrin domain should contain 6 conserved cysteine residues (Bhat et al., 2007; Chong et al., 2002) and conflicting conclusions have been asserted as to whether parasitic flatworm SFRPs satisfy this requirement (Armstrong et al., 2025; Koziol et al., 2016; Riddiford and Olson, 2011). Our alignments predict that all 6 cysteine residues are present, however, the 6th residue is displaced by three animo acids in flatworms but not humans (Fig. S5). The three additional amino acids are also present in free living *S. mediterranea* and *Smed-sfrp1* is generally accepted as a Wnt antagonist. While planarian *sfrp* paralogs show complex expression patterns (Gurley et al., 2010), *Smed-sfrp1* is an anterior marker that robustly responds to Wnt inhibition and loss of posterior identity (Doddihal et al., 2024; Hill and Petersen, 2018; Reuter et al., 2015; Scimone et al., 2016; Sureda-Gómez et al., 2015). RNAi of *Smed-sfrp1* shifts the gradient of Smed-βCAT1 protein expression anteriorly supporting *Smed-sfrp1* function as a Wnt antagonist (Stückemann et al., 2017). However, other Wnt antagonists such as *Smed-notum* demonstrate much clearer evidence of Wnt inhibition. *Smed-notum* RNAi results in tail regeneration in place of heads (Petersen and Reddien, 2011) as opposed to *Smed-βcat1* RNAi, which results in head regeneration in place of tails (Gurley et al., 2008; Iglesias et al., 2008; Petersen and Reddien, 2008). Thus, it remains possible that a muted or more ambiguous role in Wnt signaling by *sfrp1* is a shared feature in free-living and parasitic flatworms.

In addition to GR maintenance, the head negatively regulates both proliferation in the GR and proglottid regeneration in a dose-dependent and distance-dependent manner with increased proliferation farther from the head. This observation suggests that the head may be the source of growth inhibitors that diffuse or are differentially received along the A-P axis of the GR. We find that at least one posterior-enriched factor, *βcat1*, is necessary for stem cell maintenance in the GR. Knockdown of *βcat1* results in a dramatic inhibition of growth, proglottid regeneration and ultimately death. Recently, a study in the liver fluke, *Fasciola hepatica,* demonstrated that RNAi of *Fhep-βcat1* resulted in stunted juvenile growth, decreased proliferation and worm death (Armstrong et al., 2025), phenocopying our observations. Thus, roles for *βcat1* in regulating stem cell proliferation and/or survival may be a common theme in parasitic flatworms as it is in many metazoans as well as in neoplastic transformations (Mohammed et al., 2016; Steinhart and Angers, 2018) .

In addition to canonical Wnt signaling, β-catenin proteins have additional roles in cell adhesion through linking cadherins with the actin cytoskeleton via α-catenin. These two functions have been reported in many but not all species. In *S. mediterranea,* there is complete separation of function by two catenin paralogs: Smed-βCAT1 mediates Wnt signaling whereas Smed-βCAT2 mediates cell adhesion (Chai et al., 2010; Su et al., 2017). Accordingly, Smed-βCAT1 does not have α-catenin binding sites (Chai et al., 2010; Su et al., 2017). The presence/absence of α-catenin binding sites in βCAT1 from tapeworms is more ambiguous. Previously, a likely α-catenin binding region demarcated by 10 putative critical residues within a 26 amino acid span was identified for βCAT1 and βCAT2 in flatworms (Montagne et al., 2019). The 10 residues were identified as necessary for α-catenin binding to mammalian plakoglobin and/or βcatenin using alanine scanning mutagenesis (Aberle et al., 1996; Pokutta and Weis, 2000). When compared to human βcatenin (CTNB1), we and others find strong conservation of this α-catenin binding region in βCAT2 from multiple flatworms (Fig. S3B) (Montagne et al., 2019). While Smed-βCAT1 is clearly very divergent at this site, two tapeworms (*H. diminuta* and *E. multilocularis*) show more similarity to the human reference (Fig. S3B) (Montagne et al., 2019). Thus, we cannot rule out the possibility that βCAT1 in tapeworms functions in both Wnt signaling and cell adhesion, unlike their free-living counterparts. Future studies investigating the biochemical interactions and functional roles of all

βcatenin paralogs will help resolve the mechanisms regulating stem cell maintenance in parasitic flatworms.

The role of *βcat1* in posterior identity is well conserved across many taxa (Petersen and Reddien, 2009). In planarian species that are deficient in head regeneration, knockdown of *βcat1* alone can rescue head regeneration indicating that failure to regenerate the head in wild type worms was due to the inability to overcome the posteriorizing effects of *βcat1* (Liu et al., 2013; Sikes and Newmark, 2013; Umesono et al., 2013). *H. diminuta* cannot regenerate its head and we initially assumed that tapeworm *βcat1* would be acting in a homologous fashion to planarians. Because *βcat1* is required for stem cell maintenance in *H. diminuta,* potential roles in posteriorization could not be uncovered. It remains possible that Wnt signaling is necessary to maintain GR posterior identity in *H. diminuta*. Extensive RNAi manipulations of Wnt signaling components that are beyond the scope of this study will help reveal a more holistic understanding of Wnt signaling in this system. However, tapeworms and planarians do differ in that *Smed-βcat1* is not necessary for stem cell maintenance.

The differences in utilization of *βcat1* between different species of platyhelminths is potentially very interesting. Perhaps segregating functions in posteriorization vs. stem cell maintenance in *S. mediterranea* has enabled more nimble remodeling of axes that makes this species so remarkable at regenerating from almost any amputated fragment. In intestinal tapeworms, the head contains suckers that are necessary for attachment without which the tapeworm will simply be extruded with the feces. Thus, maintenance of the head and proglottid regeneration should not be easily decoupled in tapeworms. Considering the wider role for βcatenin in regulating stem cell proliferation and survival across metazoa, it would be easy to suppose that planarian phenotype is divergent. However, studies in the acoel *Hofstenia miamia*, a representative of a sister taxa to all bilaterians, show that RNAi of *Hmia-βcat1* is necessary for maintaining posterior identity but functions in regulating stem cells, proliferation, or growth were not reported (Srivastava et al., 2014; Tewari et al., 2019). Considering that *Hmia-βcat1* RNAi experiments were performed in the context of regeneration, inhibition of growth is unlikely to have been missed with the caveat the RNAi cannot be fully penetrant. Thus, there is evidence that the planarian phenotype is ancestral.

A deeper understanding of how catenin paralogs have evolved across platyhelminths and how they have functionally specialized will be illuminating. Such investigations would enrich our understanding of how strategies to regulate axial identity and stem cell proliferation/survival have evolved in regeneration-competent species.

Our work has revealed that a balance of opposing signals from anterior and posterior ends of the GR are necessary for proper regeneration. It makes intuitive sense that initiation of proglottids must be inhibited close to the head if the GR is to be maintained as an unsegmented tissue. A recent study from the mouse bile duct tapeworm, *Hymenolepis microstoma,* has described discrete expression of Wnt and Hedgehog signaling components in a signaling quartet (SQ) within the transition zone from GR to fully elaborated proglottids (Jarero et al., 2024). It is possible the SQ initiates proglottid formation and represents the unknown X factor predicted by our study. How the SQ responds to head-dependent signals and vice versa is currently unknown and warrants future investigation.

Our study also shows that regulation of proliferation dynamics is dependent on signals from the head. Why should the head provide anti-proliferation signals at all? One intriguing possibility is that distinct subpopulations of stem cells within the GR respond differentially to signals from the head. Such signals may affect the balance of self-renewal vs. differentiation. Alternatively, a slow-cycling pluri- or multi-potent subpopulation of stem cells may require these head-dependent signals. There is already evidence for different cycling rates in stem cells of parasitic flatworms (Herz et al., 2024; Wang et al., 2018) . In this study, we observed that amputations made progressively closer to the head inhibited regeneration until enough posterior GR tissue was removed, which restored competence to regenerate. Perhaps the anterior portion of the GR contains the minimal cohort of stem cells required to regenerate the GR and seed new proglottids. These anterior stem cells may represent a slow-cycling population with greater potency. These ideas are highly speculative, but investigating how head-dependent signals impact stem cell subpopulations in the GR may shed light on the regulation of stem cell potency in tapeworms and potentially other species.

Materials and Methods

Animal care and use

The life cycle of *H. diminuta* was maintained in house using mealworm beetles (*Tenebrio molitor*) and Sprague-Dawley rats for the larval and adult stages respectively. Rats were fed 200-400 infective cysticercoids by oral gavage in ~0.5 mL 0.85% NaCl. Typically, adult tapeworms were collected 6 days post infection by euthanizing infected rats in a CO_2 chamber and flushing the small intestine with 1X Hanks Balanced Salt Solution (HBSS: 21-023-CV; Corning). Rodent care was performed in accordance with protocols approved by the Institutional Animal Care and Use Committee (IACUC) of the University of Georgia (A2023 10-019-Y1-A0).

In vitro parasite culture

Adult tapeworms or amputated fragments were grown in vitro in biphasic cultures as described before (Rozario et al., 2019). 2.5X MEM essential amino acids (M5550; Sigma-Aldrich) was added to the liquid culture: Working Hanks 4 (WH4: HBSS/4 g/L glucose/antibiotic-antimycotic). This ameliorated inconsistencies between batches of blood used for culturing but was not strictly necessary.

In situ hybridization and other staining

Heat-kills were performed by swirling tapeworms in 75°C water for a few seconds before fixing (4% formaldehyde in Phosphate Buffered Saline with 0.3% TritonX-100 (PBSTx)) for 30 min-2 hr at room temperature or overnight at 4°C. Worms were either dehydrated into methanol and stored (-30°C) or used directly for staining. For simple phenotyping of growth and regeneration, worms were stained in 1 µg/mL DAPI (D9542; Sigma-Aldrich)/PBSTx overnight at 4°C and cleared in mounting solution (80% glycerol/10 mM Tris pH7.5/ 1 mM EDTA) overnight before mounting and imaging. Previously published methods were employed for in situ hybridization (Rozario et al., 2019) and immunostaining (Rozario and Newmark, 2015). Anti-Syn antibodies (3C11; Developmental Studies Hybridoma Bank) were used at 1:200 with Tyramide Signal Amplification (TSA).

F-*ara*-EdU uptake and staining

F-*ara*-EdU pulses were performed in 0.1 µM F-*ara*-EdU (T511293; Sigma-Aldrich)/1% DMSO/WH4 at 37°C for 1 hr. Staining was performed as previously described (Ishan et al., in press) with the following specifics: 1) 15 min proteinase-K digestion and 2) 10 min TSA reaction.

Imaging and image processing

Confocal imaging was performed on a Zeiss LSM 900 with the following objectives: 20X/Plan-Apochromat/0.8 M27/FWD=0.55mm and 63X/Plan-Apochromat/1.40 Oil DIC M27. WISH and DAPI-stained worms were imaged on a Zeiss AxioZoom V16 Microscope. Fiji (Schindelin et al., 2012) was used for brightness/contrast adjustments, maximum-intensity projections and measurements of lengths, areas, and numbers of proglottids. F-*ara*-EdU+ cells were quantified using Imaris (Oxford Instruments) spot finder as previously described (Ishan et al., in press) .

RNAi

To perform knockdowns, tapeworms were microinjected with dsRNA (1-1.5 µg/µl in HBSS), 2 mm anterior fragments were amputated 3 days later and cultured in vitro. Injections were performed using a Femtojet 4i (Eppendorf) at 500 hPa for 0.3-1s. dsRNA was synthesized as previously described (Rouhana et al., 2013) from ~1 kb PCR products from cDNA cloned into pJC53.2 vector (Collins et al., 2010). Experimenters were blinded to the dsRNA used throughout microinjections, staining and image analysis.

qRT-PCR

To exclude genomic DNA, primers were designed to flank introns or span an intron-exon junction. Amplicon range was 133-277 bp. All primers were tested on cDNA +/- reverse transcriptase and gel electrophoresis to confirm the presence of a single product. Primer efficiencies were calculated from 2-fold serial dilutions of cDNA.

For RNA extractions, 3 mm anteriors from 4-5 worms were cut, submerged in 200 µL TRIzol Reagent (15596026; Invitrogen) and processed according to manufacturer's instructions with these exceptions: 1) samples were homogenized with a motorized pestle twice in a semi-solid state then centrifuged at >12K RCF for 5 min to obtain 180 µL clean supernatant, 2) RNA pellets were washed twice with 75% ethanol-DEPC and 3); pellets were resuspended in 40 µL nuclease-free

water. DNAse (M6101; Promega) treatment was performed for 1 hr at 37°C. RNA was cleaned using RNA Clean & Concentrator-5 kit (R1016; Zymo Research) and the concentration measured on a Nanodrop spectrophotometer. cDNA synthesis was performed, according to manufacturer's protocol, using Oligo$(dT)_{20}$ primers and iScript Select cDNA Synthesis Kit (1708897; Bio-Rad) with undiluted RNA. cDNA was further diluted with 5-25 µL nuclease-free water depending on the number of reactions needed.

qRT-PCR was performed using GoTaq MasterMix (A6001; Promega) according to manufacturer's instructions and scaled to 25 µL reactions with 2 µL cDNA template for each of 3 technical replicates. Each reaction had 0.4 µM primer pairs, 0.3 µM CXCR in 1X master mix. 7500 Real Time PCR System (Applied Biosystems) was used for 40 amplification cycles: 15 s at 95°C and 1 min at 60°C. Relative gene expression change was calculated using the PFAFFL equation (Hellemans et al., 2007; Vandesompele et al., 2002) to account for different primer efficiencies. Internal normalization was done on the geometric mean of two previously published standards: *60S ribosomal protein L13* (*60Srpl13*) and *myosin heavy chain* (*mhc*) (Rozario et al., 2019) .

Statistical Analysis

Graph Pad Prism 10 was used for all statistical analyses. All experiments were repeated at least twice. Error bars, statistical tests, number of replicates (N) and sample sizes (n) are indicated in corresponding figure legends. P-values: ns = not significant, * = $p<0.05$, **=$p<0.01$, ***=$p<0.001$, ****=$p<0.0001$.

Acknowledgements

We are sincerely thankful to Phil Newmark and Melanie Issigonis (Morgridge Institute for Research, WI). Phil's unwavering support in the initialization of these projects and continued advice was instrumental in our success. We are also grateful for Melanie's critical evaluation of our manuscript and valuable feedback. We thank the Biomedical Microscopy Core at the University of Georgia, Athens, GA for necessary microscopy services.

Competing interests

No conflicts to report.

Funding

This work was funded by a National Institute of Allergy and Infectious Disease (NIAID) grant (DP2 AI 154416-01) to Tania Rozario.

Data and resource availability

All relevant data and resources can be found within the article and its supplementary information. Primers and transcripts used are listed in Table S2. All source data is provided in Table S3.

References

Aberle, H., Schwartz, H., Hoschuetzky, H. and Kemler, R. (1996). Single Amino Acid Substitutions in Proteins of the armadillo Gene Family Abolish Their Binding to α-Catenin (∗). *J. Biol. Chem.* **271**, 1520–1526.

Armstrong, R., Marks, N. J., Geary, T. G., Harrington, J., Selzer, P. M. and Maule, A. G. (2025). Wnt/β-catenin signalling underpins juvenile *Fasciola hepatica* growth and development. *PLOS Pathog.* **21**, e1012562.

Bely, A. E. and Nyberg, K. G. (2010). Evolution of animal regeneration: re-emergence of a field. *Trends in Ecology & Evolution* **25**, 161–170.

Bhat, R. A., Stauffer, B., Komm, B. S. and Bodine, P. V. N. (2007). Structure–Function analysis of secreted frizzled-related protein-1 for its Wnt antagonist function. *J. Cell. Biochem.* **102**, 1519–1528.

Blum, M., Chang, H.-Y., Chuguransky, S., Grego, T., Kandasaamy, S., Mitchell, A., Nuka, G., Paysan-Lafosse, T., Qureshi, M., Raj, S., et al. (2020). The InterPro protein families and domains database: 20 years on. *Nucleic Acids Res.* **49**, D344–D354.

Bovolenta, P., Esteve, P., Ruiz, J. M., Cisneros, E. and Lopez-Rios, J. (2008). Beyond Wnt inhibition: new functions of secreted Frizzled-related proteins in development and disease. *J. Cell Sci.* **121**, 737–746.

Chai, G., Ma, C., Bao, K., Zheng, L., Wang, X., Sun, Z., Salò, E., Adell, T. and Wu, W. (2010). Complete functional segregation of planarian β-catenin-1 and -2 in mediating Wnt signaling and cell adhesion. *The Journal of biological chemistry* **285**, 24120–24130.

Chong, J. M., Üren, A., Rubin, J. S. and Speicher, D. W. (2002). Disulfide Bond Assignments of Secreted Frizzled-related Protein-1 Provide Insights about Frizzled Homology and Netrin Modules. *J. Biol. Chem.* **277**, 5134–5144.

Collins, J. J., Hou, X., Romanova, E. V., Lambrus, B. G., Miller, C. M., Saberi, A., Sweedler, J. V. and Newmark, P. A. (2010). Genome-wide analyses reveal a role for peptide hormones in planarian germline development. *PLoS biology* **8**, e1000509.

Doddihal, V., Mann, F. G., Ross, E. J., McKinney, M. C., Guerrero-Hernández, C., Brewster, C. E., McKinney, S. A. and Alvarado, A. S. (2024). A PAK family kinase and the Hippo/Yorkie pathway modulate WNT signaling to functionally integrate body axes during regeneration. *Proc. Natl. Acad. Sci.* **121**, e2321919121.

Goodchild, C. G. (1958). Transfaunation and Repair of Damage in the Rat Tapeworm, *Hymenolepis diminuta*. *The Journal of parasitology* **44**, 345–351.

Gurley, K. A., Rink, J. C. and Alvarado, A. S. (2008). β-catenin defines head versus tail identity during planarian regeneration and homeostasis. *Science* **319**, 323–327.

Gurley, K. A., Elliott, S. A., Simakov, O., Schmidt, H. A., Holstein, T. W. and Alvarado, A. S. (2010). Expression of secreted Wnt pathway components reveals unexpected complexity of the planarian amputation response. *Developmental biology* **347**, 24–39.

Hellemans, J., Mortier, G., Paepe, A. D., Speleman, F. and Vandesompele, J. (2007). qBase relative quantification framework and software for management and automated analysis of real-time quantitative PCR data. *Genome Biol.* **8**, R19.

Herz, M., Zarowiecki, M., Wessels, L., Pätzel, K., Herrmann, R., Braun, C., Holroyd, N., Huckvale, T., Bergmann, M., Spiliotis, M., et al. (2024). Genome-wide transcriptome analysis of *Echinococcus multilocularis* larvae and germinative cell cultures reveals genes involved in parasite stem cell function. *Front. Cell. Infect. Microbiol.* **14**, 1335946.

Hill, E. M. and Petersen, C. P. (2018). Positional information specifies the site of organ regeneration and not tissue maintenance in planarians. *eLife* **7**, e02238.

Holly, V. L., Widen, S. A., Famulski, J. K. and Waskiewicz, A. J. (2014). Sfrp1a and Sfrp5 function as positive regulators of Wnt and BMP signaling during early retinal development. *Dev. Biol.* **388**, 192–204.

Iglesias, M., Gomez-Skarmeta, J. L., Saló, E. and Adell, T. (2008). Silencing of *Smed-βcatenin1* generates radial-like hypercephalized planarians. *Development* **135**, 1215–1221.

Ishan, M., Skipper, I. R. and Rozario, T. (2025). Combined fluorescent in situ hybridization and F-ara-EdU staining on whole mount *Hymenolepis diminuta*. *Biol. Methods Protoc.* bpaf011. (in press)

Jarero, F., Baillie, A., Riddiford, N., Montagne, J., Koziol, U. and Olson, P. D. (2024). Muscular remodeling and anteroposterior patterning during tapeworm segmentation. *Dev. Dyn.* **253**: 998–1023.

Koziol, U., Jarero, F., Olson, P. D. and Brehm, K. (2016). Comparative analysis of Wnt expression identifies a highly conserved developmental transition in flatworms. *BMC biology* **14**, 1.

Laumer, C. E., Hejnol, A. and Giribet, G. (2015). Nuclear genomic signals of the "microturbellarian" roots of platyhelminth evolutionary innovation. *eLife* **4**, e05503.

Leyns, L., Bouwmeester, T., Kim, S.-H., Piccolo, S. and Robertis, E. M. D. (1997). Frzb-1 Is a Secreted Antagonist of Wnt Signaling Expressed in the Spemann Organizer. *Cell* **88**, 747–756.

Liu, S. Y., Selck, C., Friedrich, B., Lutz, R., Vila-Farré, M., Dahl, A., Brandl, H., Lakshmanaperumal, N., Henry, I. and Rink, J. C. (2013). Reactivating head regrowth in a regeneration-deficient planarian species. *Nature* **500**, 81–84.

Mii, Y. and Taira, M. (2011). Secreted Wnt "inhibitors" are not just inhibitors: Regulation of extracellular Wnt by secreted Frizzled-related proteins. *Dev., Growth Differ.* **53**, 911–923.

Mohammed, M. K., Shao, C., Wang, J., Wei, Q., Wang, X., Collier, Z., Tang, S., Liu, H., Zhang, F., Huang, J., et al. (2016). Wnt/β-catenin signaling plays an ever-expanding role in stem cell self-renewal, tumorigenesis and cancer chemoresistance. *Genes Dis.* **3**, 11–40.

Montagne, J., Preza, M., Castillo, E., Brehm, K. and Koziol, U. (2019). Divergent Axin and GSK-3 paralogs in the beta-catenin destruction complexes of tapeworms. *Development genes and evolution* **11**, 1–14.

Nusse, R. and Clevers, H. (2017). Wnt/β-Catenin Signaling, Disease, and Emerging Therapeutic Modalities. *Cell* **169**, 985–999.

Petersen, C. P. and Reddien, P. W. (2008). *Smed-βcatenin-1* is required for anteroposterior blastema polarity in planarian regeneration. *Science* **319**, 327–330.

Petersen, C. P. and Reddien, P. W. (2009). Wnt signaling and the polarity of the primary body axis. *Cell* **139**, 1056–1068.

Petersen, C. P. and Reddien, P. W. (2011). Polarized notum activation at wounds inhibits Wnt function to promote planarian head regeneration. *Science* **332**, 852–855.

Pokutta, S. and Weis, W. I. (2000). Structure of the Dimerization and β-Catenin- Binding Region of α-Catenin. *Mol. Cell* **5**, 533–543.

Rattner, A., Hsieh, J.-C., Smallwood, P. M., Gilbert, D. J., Copeland, N. G., Jenkins, N. A. and Nathans, J. (1997). A family of secreted proteins contains homology to the cysteine-rich ligand-binding domain of frizzled receptors. *Proc. Natl. Acad. Sci.* **94**, 2859–2863.

Read, C. P. (1967). Longevity of the tapeworm, *Hymenolepis diminuta*. *J Parasitol* **53**, 1055–6.

Reddien, P. W. (2018). The Cellular and Molecular Basis for Planarian Regeneration. *Cell* **175**, 327–345.

Reuter, H., März, M., Vogg, M. C., Eccles, D., Grífol-Boldú, L., Wehner, D., Owlarn, S., Adell, T., Weidinger, G. and Bartscherer, K. (2015). β-Catenin-Dependent Control of Positional Information along the AP Body Axis in Planarians Involves a Teashirt Family Member. *Cell reports* **10**, 253–265.

Riddiford, N. and Olson, P. D. (2011). Wnt gene loss in flatworms. *Development genes and evolution* **221**, 187–197.

Rouhana, L., Weiss, J. A., Forsthoefel, D. J., Lee, H., King, R. S., Inoue, T., Shibata, N., Agata, K. and Newmark, P. A. (2013). RNA interference by feeding in vitro-synthesized double-stranded RNA to planarians: methodology and dynamics. *Dev. Dyn.* **242**, 718–730.

Rozario, T. and Newmark, P. A. (2015). A confocal microscopy-based atlas of tissue architecture in the tapeworm *Hymenolepis diminuta*. *Experimental parasitology* **158**, 31–41.

Rozario, T., Quinn, E. B., Wang, J., Davis, R. E. and Newmark, P. A. (2019). Region-specific regulation of stem cell-driven regeneration in tapeworms. *eLife* **8**, e48958.

Schindelin, J., Arganda-Carreras, I., Frise, E., Kaynig, V., Longair, M., Pietzsch, T., Preibisch, S., Rueden, C., Saalfeld, S., Schmid, B., et al. (2012). Fiji: an open-source platform for biological-image analysis. *Nat. Methods* **9**, 676–682.

Scimone, M. L., Cote, L. E., Rogers, T. and Reddien, P. W. (2016). Two FGFRL-Wnt circuits organize the planarian anteroposterior axis. *eLife* **5**, 905.

Sikes, J. M. and Newmark, P. A. (2013). Restoration of anterior regeneration in a planarian with limited regenerative ability. *Nature* **500**, 77–80.

Soria, C. L. D., Lee, J., Chong, T., Coghlan, A., Tracey, A., Young, M. D., Andrews, T., Hall, C., Ng, B. L., Rawlinson, K., et al. (2020). Single-cell atlas of the first intra-mammalian developmental stage of the human parasite *Schistosoma mansoni*. *Nat. Commun.* **11**, 6411.

Srivastava, M., Mazza-Curll, K. L., Wolfswinkel, J. C. van and Reddien, P. W. (2014). Whole-Body Acoel Regeneration Is Controlled by Wnt and Bmp-Admp Signaling. *Current biology : CB* **24**, 1107–1113.

Steinhart, Z. and Angers, S. (2018). Wnt signaling in development and tissue homeostasis. *Development* **145**, dev146589.

Stückemann, T., Cleland, J. P., Werner, S., Vu, H. T.-K., Bayersdorf, R., Liu, S.-Y., Friedrich, B., Jülicher, F. and Rink, J. C. (2017). Antagonistic Self-Organizing Patterning Systems Control Maintenance and Regeneration of the Anteroposterior Axis in Planarians. *Developmental cell* **40**, 248-263.e4.

Su, H., Sureda-Gomez, M., Rabaneda-Lombarte, N., Gelabert, M., Xie, J., Wu, W. and Adell, T. (2017). A C-terminally truncated form of β-catenin acts as a novel regulator of Wnt/β-catenin signaling in planarians. *PLoS Genet.* **13**, e1007030.

Sureda-Gómez, M., Pascual-Carreras, E. and Adell, T. (2015). Posterior Wnts Have Distinct Roles in Specification and Patterning of the Planarian Posterior Region. *International journal of molecular sciences* **16**, 26543–26554.

Tewari, A. G., Owen, J. H., Petersen, C. P., Wagner, D. E. and Reddien, P. W. (2019). A small set of conserved genes, including *sp5* and *Hox*, are activated by Wnt signaling in the posterior of planarians and acoels. *PLoS Genet.* **15**, e1008401.

Umesono, Y., Tasaki, J., Nishimura, Y., Hrouda, M., Kawaguchi, E., Yazawa, S., Nishimura, O., Hosoda, K., Inoue, T. and Agata, K. (2013). The molecular logic for planarian regeneration along the anterior-posterior axis. *Nature* **500**, 73–76.

Üren, A., Reichsman, F., Anest, V., Taylor, W. G., Muraiso, K., Bottaro, D. P., Cumberledge, S. and Rubin, J. S. (2000). Secreted Frizzled-related Protein-1 Binds Directly to Wingless and Is a Biphasic Modulator of Wnt Signaling*. *J. Biol. Chem.* **275**, 4374–4382.

Valenta, T., Hausmann, G. and Basler, K. (2012). The many faces and functions of β-catenin. *EMBO J.* **31**, 2714–2736.

Vandesompele, J., Preter, K. D., Pattyn, F., Poppe, B., Roy, N. V., Paepe, A. D. and Speleman, F. (2002). Accurate normalization of real-time quantitative RT-PCR data by geometric averaging of multiple internal control genes. *Genome Biol.* **3**, research0034.1.

Wang, S., Krinks, M., Lin, K., Luyten, F. P. and Moos, M. (1997). Frzb, a Secreted Protein Expressed in the Spemann Organizer, Binds and Inhibits Wnt-8. *Cell* **88**, 757–766.

725 **Wang, B., Lee, J., Li, P., Saberi, A., Yang, H., Liu, C., Zhao, M. and Newmark, P. A.**
726 (2018). Stem cell heterogeneity drives the parasitic life cycle of *Schistosoma mansoni*. *eLife*
727 **7**, e35449.

728

Figure legends

Fig. 1. The germinative region (GR) regenerates after a single amputation. (A) DAPI-stained images of anterior fragments cut within the GR (0.5 mm) or outside of it (2 mm) at 15 dpa. Quantification of growth in length and number of proglottids regenerated at 15 dpa. N=3, n= 6-10 per condition; t-test. (B) DAPI-stained image of 0.5 mm anterior fragment at 15 dpa showing regenerated GR. Yellow arrowhead marks the first proglottid. Quantification of GR lengths from A; t-test. (C) Quantification of proglottids regenerated and length every 2 days from 0.5 mm vs. 2 mm anterior fragments. Change in proglottids was fitted with a simple linear regression and showed 14-15 proglottids regenerated per day. Change in length was fitted with a nonlinear curve as each proglottid increases in length. n=5-7 fragments per group per timepoint. (D) WISH for transcripts with A-P polarized expression patterns 3 days after acclimation to in vitro culture (uncut, n = 7-10 per transcript) then amputated at 0.5 mm and stained at 0 dpa (n= 7-8 per transcript) and 10 dpa (n= 5-13 per transcript). Asterisks mark pigmented debris that adhered to cut ends. Error bars= SD.

Fig. 2. Serial amputation within the GR negatively affects regenerative ability. (A) Scheme for serial amputation within the GR. (B-C) GR lengths and percentage of GR retained compared to uncut whole worms at 0 dpa. n=7-10 per timepoint per experiment. (D) DAPI-stained regenerates 18 dpa for each cut. (E-F) Quantification of regeneration success rate and number of proglottids regenerated (n= 8-10 per timepoint per experiment). Error bars= SD; t-test.

Fig. 3. The head inhibits proglottid regeneration and cell proliferation. (A) DAPI-stained regenerates from 0.5 mm amputations +/- head at 15 dpa. Quantification of proglottids regenerated from a representative experiment. n= 7; t-test. (B) Confocal micrographs from maximum intensity projections of +/- head worms at 3 dpa immunostained for neuronal marker SYN after a 1 hr pulse of F-*ara*-EdU to label proliferating cells. Quantification of the density of proliferating cells within the GR from a representative experiment. Each sample was normalized to the mean proliferation density in the corresponding +head group. n= 5-6 per group per timepoint; t-test. (C-D) Maximum intensity projections of worm anteriors after 1 hr pulse of F-*ara*-EdU either with the head (C) or -head 3 dpa (D). Yellow dotted lines represent 200 μm-wide regions used for quantification of

760 proliferation density. H= head. Quantification across 3 cohorts, n=11 and 13; one-way ANOVA
761 with Dunnett's multiple testing correction. Error bars= SD.
762
763 **Fig. 4. Effect of head or head-adjacent amputations on proliferation and regeneration.** (A)
764 Scheme for results shown in B-C and Fig. S2. Step 1: Four amputation schemes were tested: intact
765 head (+head), transverse cut through half the head while retaining the brain (½ head), full head
766 amputation (-head) and cut 0.5 mm from the anterior into the GR (-0.5 mm). Step 2: all worms
767 were amputated posteriorly to obtain 2 mm fragments. Step 3: fragments were grown in vitro for
768 14 days. Step 4-5: regenerates were collected and recut to obtain 2 mm anterior fragments that
769 were cultured in vitro while the posteriors were fixed and stained with DAPI to measure the
770 number of proglottids regenerated. (B) Quantification of proglottids regenerated. All samples were
771 normalized to the mean of the +head worms set to 100%. Bars indicate the means from 2-3
772 experiments for all samples after cut 1 and only for samples with visible GRs for cut 2-4. Fully
773 proglottidized worms without a GR are represented with a red dot. (C) Percentage of regenerates
774 that still maintained a visible GR from B. (D) After cut 4, proglottids regenerated from +head and
775 ½ head samples from one experiment were plotted against the area of the head remaining measured
776 from DAPI stained worms. Linear regression fitted. (E-F) Quantification of F-*ara*-EdU+ cells
777 normalized to area within the GR 3 dpa. All samples were normalized to the mean of the +head
778 worms set to 100%. Means from 3-4 experiments analyzed with two-way ANOVA (mixed model)
779 and Tukey's multiple corrections test (E). All pooled data from analyzed with one-way ANOVA
780 compared to +head with Dunnett's multiple comparison test (n= 21-28). Error bars= SD.
781
782 **Fig. 5. *βcat1* is a posterior-biased factor that is necessary to maintain the cycling stem cell**
783 **population in the GR.** (A) Schematic and WISH of *βcat1* expression at the GR from a wild type
784 6-day-old adult. (B) DAPI-stained 2 mm anterior regenerates after single injection of dsRNA at 7
785 dpa. (C) Quantification of worm lengths after RNAi at 7 dpa. Bars show means and grey circles
786 represent individual worms. N= 3, n= 23-24 per group; one-way ANOVA with Dunnett's multiple
787 comparison test. (D) qRT-PCR from 3 RNAi experiments. Target expression normalized to two
788 endogenous controls and compared to *GFP* RNAi set at 1 (dotted line). (E) Representative
789 maximum intensity confocal projections at the GR stained after 1 hr F-*ara*-EdU uptake. Dotted
790 yellow lines are the worm outlines. Quantification of F-*ara*-EdU+ cells normalized to area within

an 800 µm-wide cropped region directly posterior to the head at 6-7 dpi. All samples were normalized to the mean of *GFP* RNAi worms set to 100%. Bars show means and grey circles represent individual worms. N= 3, n= 16-20 per group; one-way ANOVA with Dunnett's multiple comparison test. (F) WISH for cycling stem cell markers *mcm2* and *lbr* at 6 dpi (N=3). Error bars= SD.

Fig. 6. *sfrp* is an anterior-biased factor that regulates GR length. (A) Schematic and WISH of *sfrp* expression at the GR from a wild type 6-day-old adult. (B) RNAi scheme for C-F. Double injections of dsRNA were performed into the head and 2 mm anterior fragments were allowed to regenerate for 10-12 days. (C) Representative DAPI-stained regenerates after RNAi. (D) Quantification of proglottids regenerated after RNAi normalized to mean from *GFP* RNAi set to 100%. Bars show means and grey circles represent individual worms. N= 3, n= 25-26 per group; one-way ANOVA with Dunnett's multiple comparison test. (E) Representative DAPI-stained images showing GR lengths (between yellow arrowheads) after RNAi. (F) Quantification of GR lengths from D. Bars show means and grey circles represent individual worms; one-way ANOVA with Dunnett's multiple comparison test. (G) qRT-PCR for *sfrp* expression normalized to two endogenous controls compared +head set at 1. N=3; t-test. Error bars= SD.

Fig. 7. How amputations at increasing distance from the head influence competence to regenerate. (A) Regenerates from 0.5 mm anterior fragments were grown for 18 days then amputated a second time at 1 mm (cut A). A subset was fixed to quantify GR length and a subset was grown in vitro for 18 days. The remaining fragments were cut again to shave off ~20-25% more GR (cut B) and the process repeated successively for cut C and cut D. Darkfield images showing the live fragments before transfer to in vitro culture show that the wound site is progressively closer to the head with successive cuts. (B) GR lengths of each fragment measured from DAPI-stained 0 dpa fragments and represented as a percentage of the GR relative to uncut worms from the same cohort. N=3, n= 3-9; one-way ANOVA. (C) Percent of fragments that regenerated proglottids after 18 days from 3 experiments. Each experiment represented by the same color in B and C. (D-F) Comparisons of worm length (D), growth fold change (E) and GR length (F). N=3, n= 20 and 17; t-test. Error bars = SD.

822 **Fig. 8. Models for regeneration in *H. diminuta*.** (A) Working model for a minimal complement
823 of factors within the GR. X represents unknown factor(s) that directly/indirectly promote *βcat1*
824 activity. (B-D) Graphical representation using the working model to explain three scenarios
825 described in this study. For all: solid black activating or inhibiting arrows indicate activity in situ
826 whereas dotted grey arrows indicate the associated function without spatial reference.
827
828 **Fig. S1. Proliferation response at wound site.** Worms were amputated at 0.5 mm within the GR.
829 Fragments were analyzed at both the posterior-facing wound (Pfw) and anterior-facing wound
830 (Afw) at 1 dpa following a 1 hr pulse of F-*ara*-EdU. Proliferation density was quantified from a
831 box width of 100 μm from the cut site to capture the local proliferation response to amputation.
832 Quantification from one representative experiment is shown, n= 5-7; error bars= SD, one-way
833 ANOVA with Tukey's multiple testing correction.
834
835 **Fig. S2. How head tissues influence regeneration.** (A) Widefield fluorescent images of ½ head
836 fragments at 0 dpa stained with anti-SYN antibodies. Yellow arrowheads point to the
837 brain/cephalic ganglia. (B) GR lengths at the end of a representative serial amputation experiment.
838 n= 5-8; one-way ANOVA with Dunnett's multiple comparison test. (C) Quantification of
839 proglottids regenerated after cut 1, normalized to +head means. N=3; n=7-17; statistical
840 significance for each of 3 experiments calculated using one-way ANOVA and was the same for
841 all 3. (D) Quantification of proglottids regenerated normalized to +head means. N=2-3, n=5-16;
842 means (black circles) and statistical significance for each experiment using t-test are shown. Error
843 bars= SD.
844
845 **Fig. S3. Domain analysis of *H. diminuta* βCAT1.** (A) Sequence alignment of βCAT1 from four
846 flatworm species (*Hd: H. diminuta, Em: E. multilocularis, Sm: S. mansoni, Smed: S.*
847 *mediterranea*). The conserved DSGxxSxxx[S/T]xxxS motif for CKI/GSK-phosphorylation (red)
848 is present as are armadillo repeats (lilac). The boundaries of both domains are shown according to
849 *S. mediterranea* (Su et al., 2017). The shading indicates identical residues between 4 species (grey)
850 or 3 species (blue). The N- and C-termini are more divergent between all species. (B) Sequence
851 alignment of 26 amino acids covering a putative α-catenin binding domain previously reported
852 (Montagne et al., 2019). 10 critical residues for α-catenin binding (Aberle et al., 1996; Pokutta and

Weis, 2000) are marked by the symbol α (green). In reference to human CTNB1, dark grey shading highlights identical residues. Chemically similar residues marked in light grey for aromatic (F, Y, W, H), aliphatic (V, I, L), positively charged (R, K, H), negatively charged (D, E), polar but not charged (N, Q, T, S, Y, C) and hydrophobic (V, I, L, M, A, F, P, W, G) residues, also in reference to human CTNB1.

Fig. S4. Wild type WISH expression patterns for *βcat1* and *sfrp*. Representative micrographs spanning different stages of development in 6-day-old worms with anterior facing left.

Fig. S5. Domain analysis of *H. diminuta* SFRP. BLASTp alignment of SFRPs from flatworms and human SFRP-1,-2 and -5 as references (*Hd: H. diminuta, Em: E. multilocularis, Smed: S. mediterranea*). The frizzled domain (orange) and netrin domain (blue) are marked at the most inclusive positions reported for human SFRP1 using Interpro (Blum et al., 2020). Conserved cysteines are highlighted in yellow.

Fig. S6. Phenotypes observed after *sfrp* RNAi. (A) Scheme for RNAi with dsRNA injections throughout the GR. (B-C) Quantification of proglottid regeneration (B) and GR length (C) from two independent experiments; one-way ANOVA with Dunnett's multiple comparison test. (D) Quantification of F-*ara*-EdU+ cells normalized to area within an 800 µm-wide cropped region directly posterior to the head or to the first proglottid. Combined from single and double injections of dsRNA throughout the GR all from experiments with significant *sfrp* knockdown. All samples were normalized to the mean of *GFP* RNAi worms set to 100%. Bars show means and grey circles represent individual worms. N= 3, n= 21-23 per group; one-way ANOVA with Dunnett's multiple comparison test. (E) qRT-PCR from 3 RNAi experiments where dsRNA was injected at the scolex (Sc-biased) or throughout the GR. Expression of *sfrp* was normalized to two endogenous controls compared to *GFP* RNAi set at 1 (dotted line). Error bars= SD.

Fig. S7. Comparison of regenerates from longest (cut A) vs. shortest (cut D) fragments after re-amputation. (A) DAPI-stained regenerates at 18 dpa. (B) Proglottid regeneration at 18 dpa. N=3, n= 20 and 17; t-test, error bars = SD.

884 **Table S1. *βcatenin* paralogs.** BLASTp analysis indicates that *H. diminuta* has three *βcatenin*
885 paralogs with orthologs in other flatworms.
886
887 **Table S2. Primers and transcripts used in this study.**
888
889 **Table S3. All source data used in this study.**

Figure 1

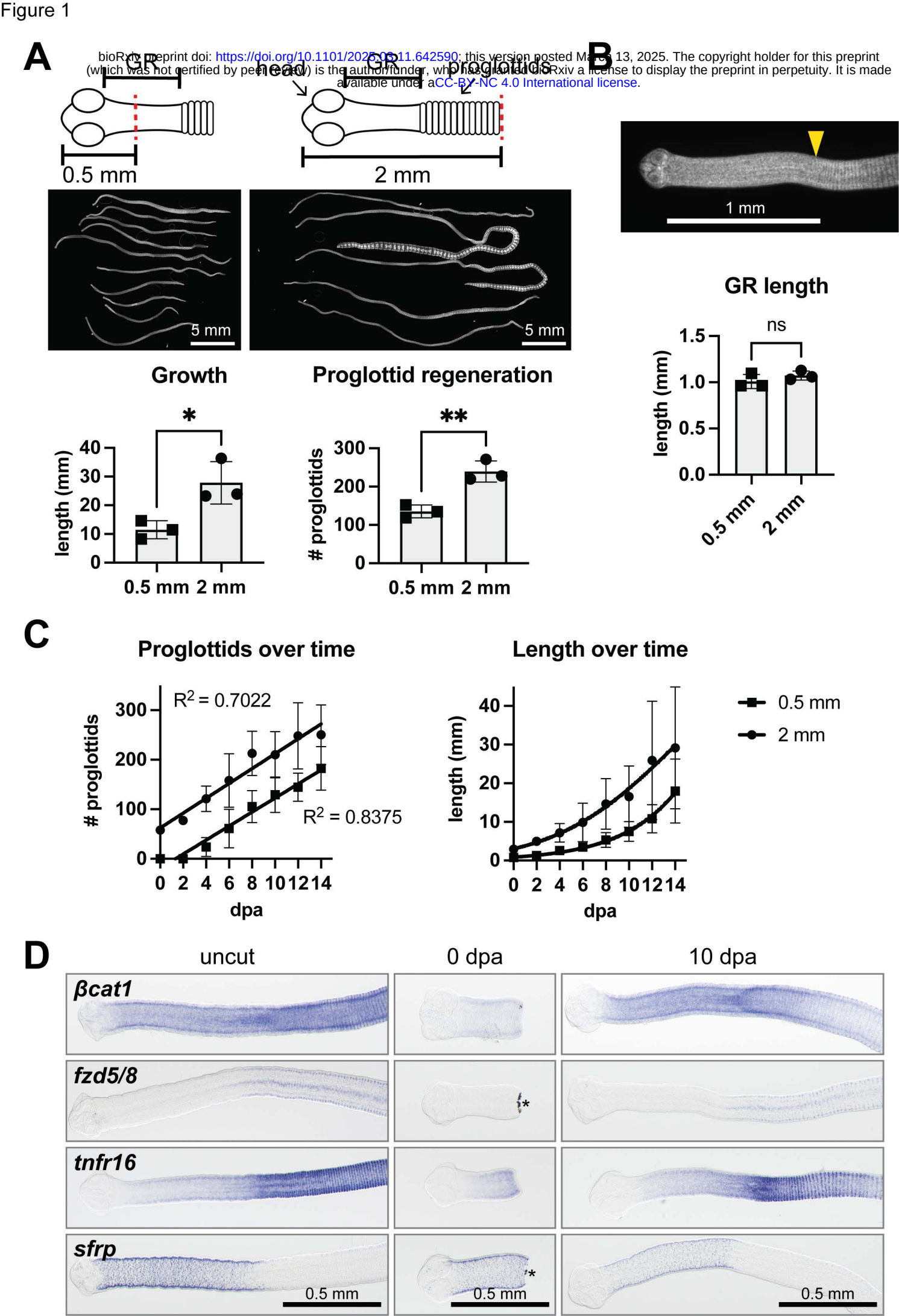

Figure 2

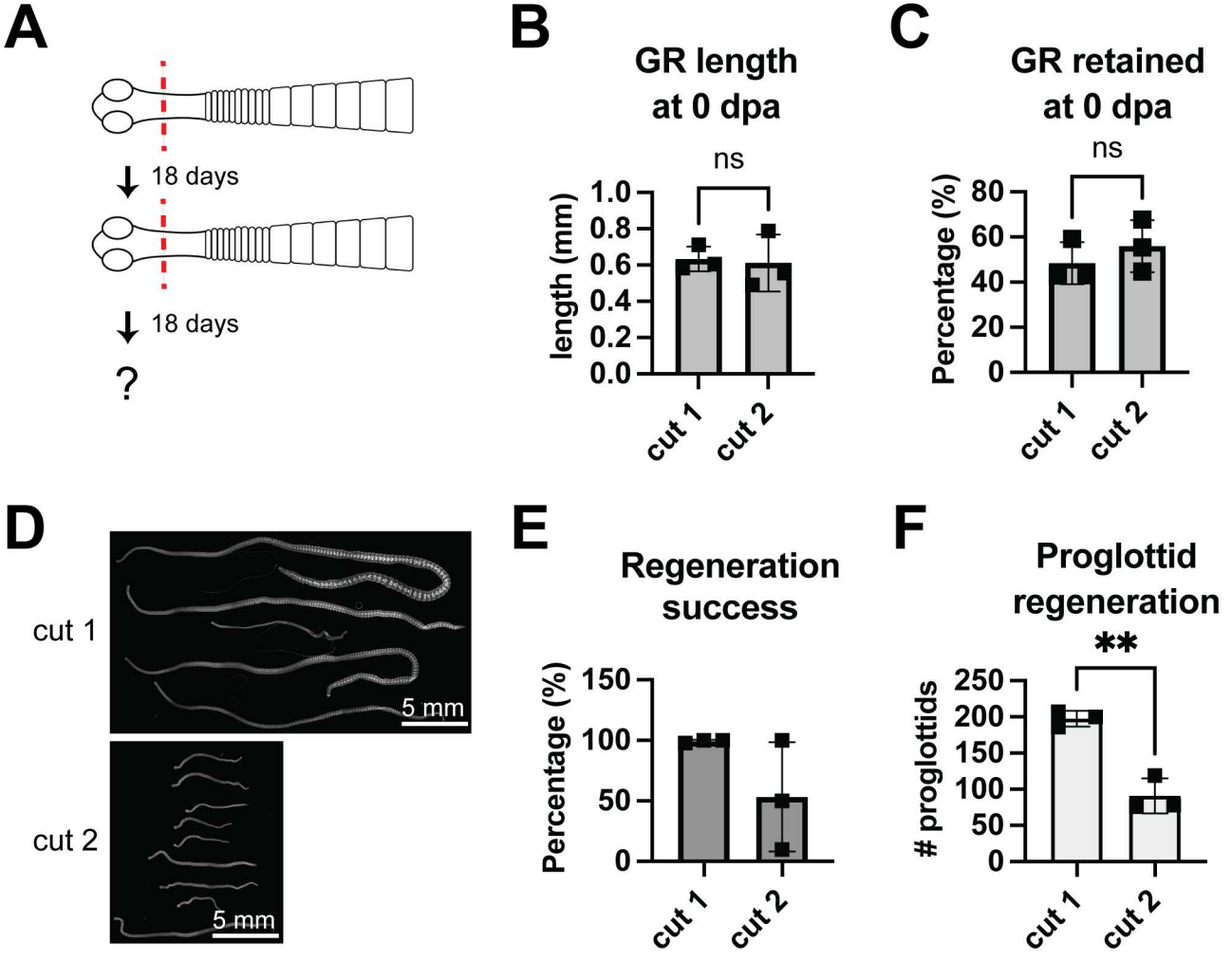
A
18 days
18 days
?
B
GR length at 0 dpa
ns
length (mm)
1.0
0.8
0.6
0.4
0.2
0.0
cut 1
cut 2
C
GR retained at 0 dpa
ns
Percentage (%)
80
60
40
20
0
cut 1
cut 2
D
cut 1
5 mm
cut 2
5 mm
E
Regeneration success
Percentage (%)
150
100
50
0
cut 1
cut 2
F
Proglottid regeneration
**
proglottids
250
200
150
100
50
0
cut 1
cut 2

Figure 3

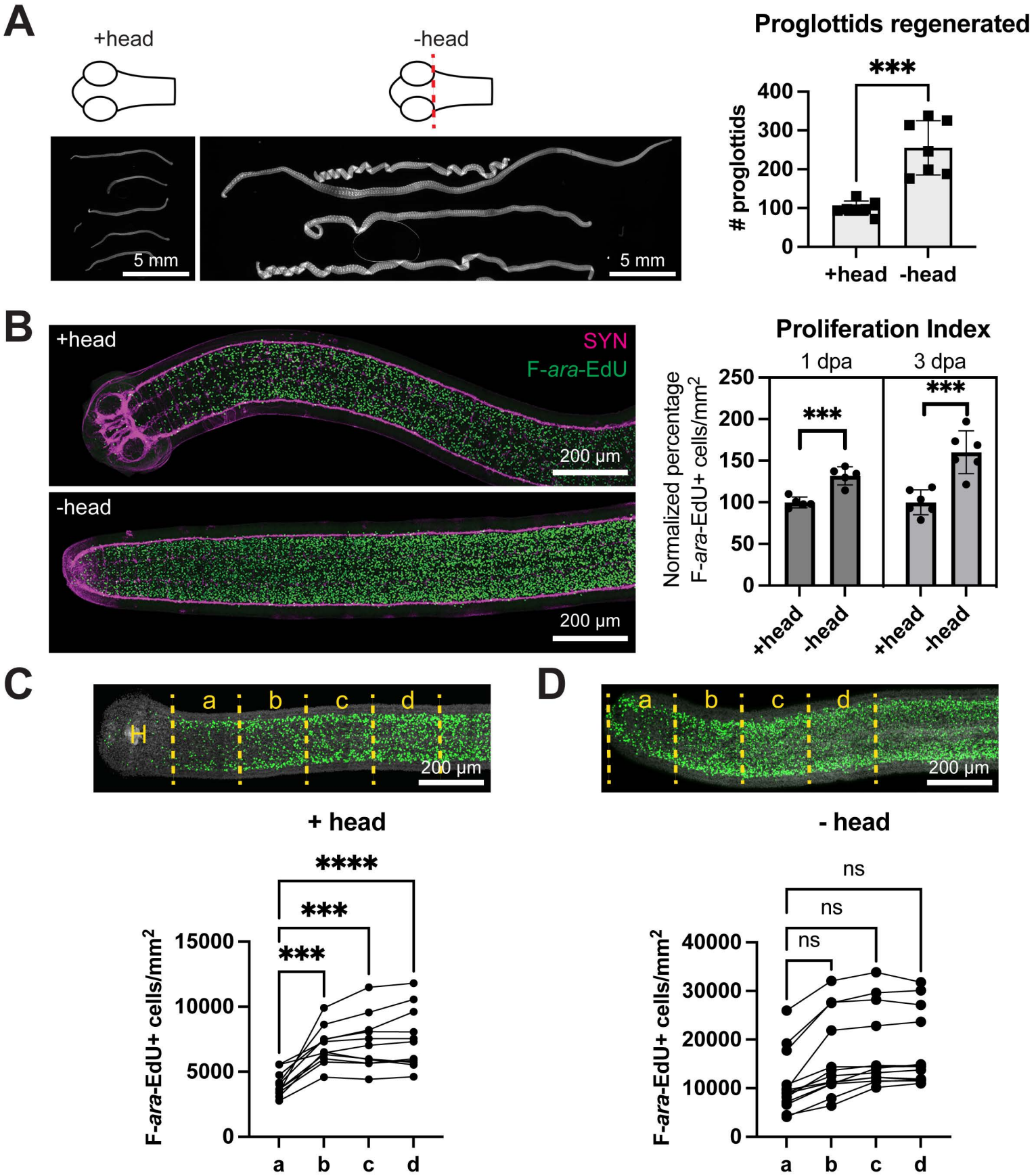
A
+head
-head
5 mm
5 mm
Proglottids regenerated
***
proglottids
400
300
200
100
0
+head
-head
B
+head
SYN
F-ara-EdU
200 µm
-head
200 µm
Proliferation Index
1 dpa
3 dpa
Normalized percentage F-ara-EdU+ cells/mm2
250
200
150
100
50
0
***
***
+head
-head
+head
-head
C
H
a
b
c
d
200 µm
+ head
****
***
***
F-ara-EdU+ cells/mm2
15000
10000
5000
0
a
b
c
d
D
a
b
c
d
200 µm
- head
ns
ns
ns
F-ara-EdU+ cells/mm2
40000
30000
20000
10000
0
a
b
c
d

Figure 4

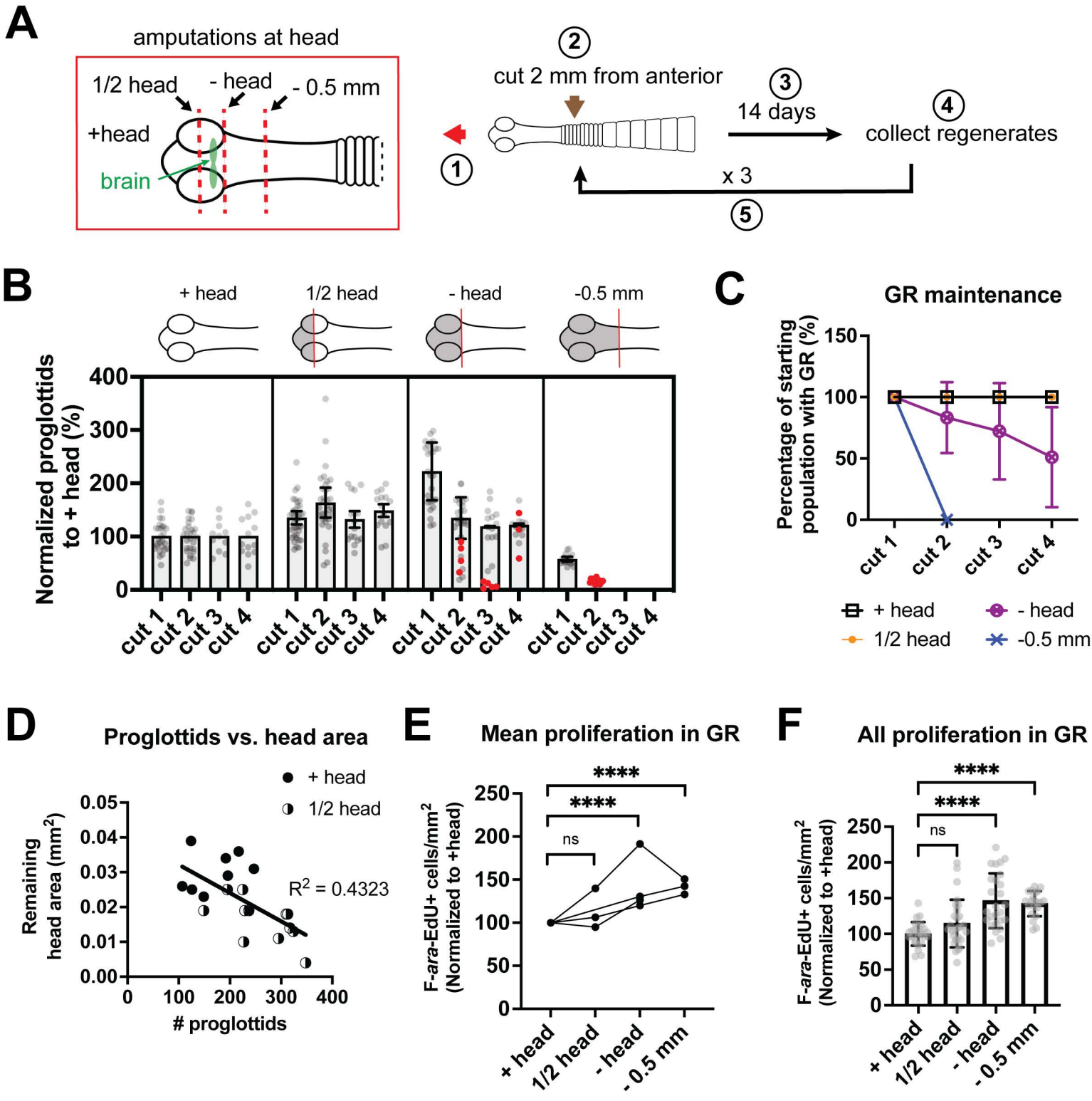
A
amputations at head
1/2 head
- head
- 0.5 mm
+head
brain
2
cut 2 mm from anterior
3
14 days
4
collect regenerates
1
x 3
5
B
+ head
1/2 head
- head
-0.5 mm
Normalized proglottids to + head (%)
400
300
200
100
0
cut 1
cut 2
cut 3
cut 4
C
GR maintenance
Percentage of starting population with GR (%)
150
100
50
0
cut 1
cut 2
cut 3
cut 4
+ head
- head
1/2 head
-0.5 mm
D
Proglottids vs. head area
+ head
1/2 head
Remaining head area (mm²)
0.05
0.04
0.03
0.02
0.01
0.00
R² = 0.4323
0
100
200
300
400
proglottids
E
Mean proliferation in GR
F-ara-EdU+ cells/mm² (Normalized to +head)
****
****
ns
250
200
150
100
50
0
+ head
1/2 head
- head
-0.5 mm
F
All proliferation in GR
F-ara-EdU+ cells/mm² (Normalized to +head)
****
****
ns
250
200
150
100
50
0
+ head
1/2 head
- head
-0.5 mm

Figure 5

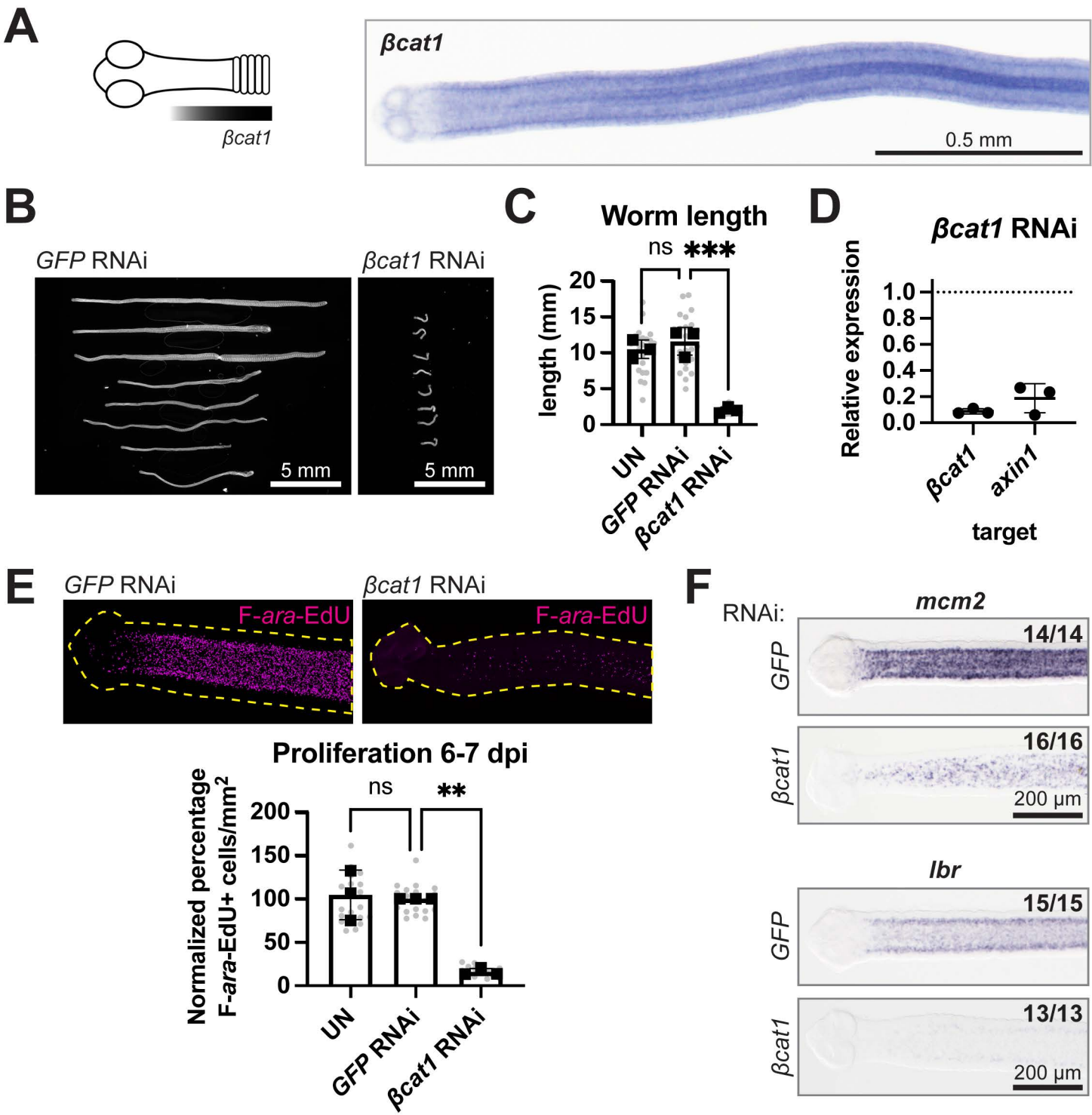
A
βcat1
βcat1
0.5 mm
B
GFP RNAi
βcat1 RNAi
5 mm
5 mm
C
Worm length
ns
***
length (mm)
20
15
10
5
0
UN
GFP RNAi
βcat1 RNAi
D
βcat1 RNAi
Relative expression
1.0
0.8
0.6
0.4
0.2
0.0
βcat1
axin1
target
E
GFP RNAi
βcat1 RNAi
F-ara-EdU
F-ara-EdU
Proliferation 6-7 dpi
ns
**
Normalized percentage F-ara-EdU+ cells/mm²
200
150
100
50
0
UN
GFP RNAi
βcat1 RNAi
F
RNAi:
mcm2
GFP
14/14
βcat1
16/16
200 µm
lbr
GFP
15/15
βcat1
13/13
200 µm

Figure 6

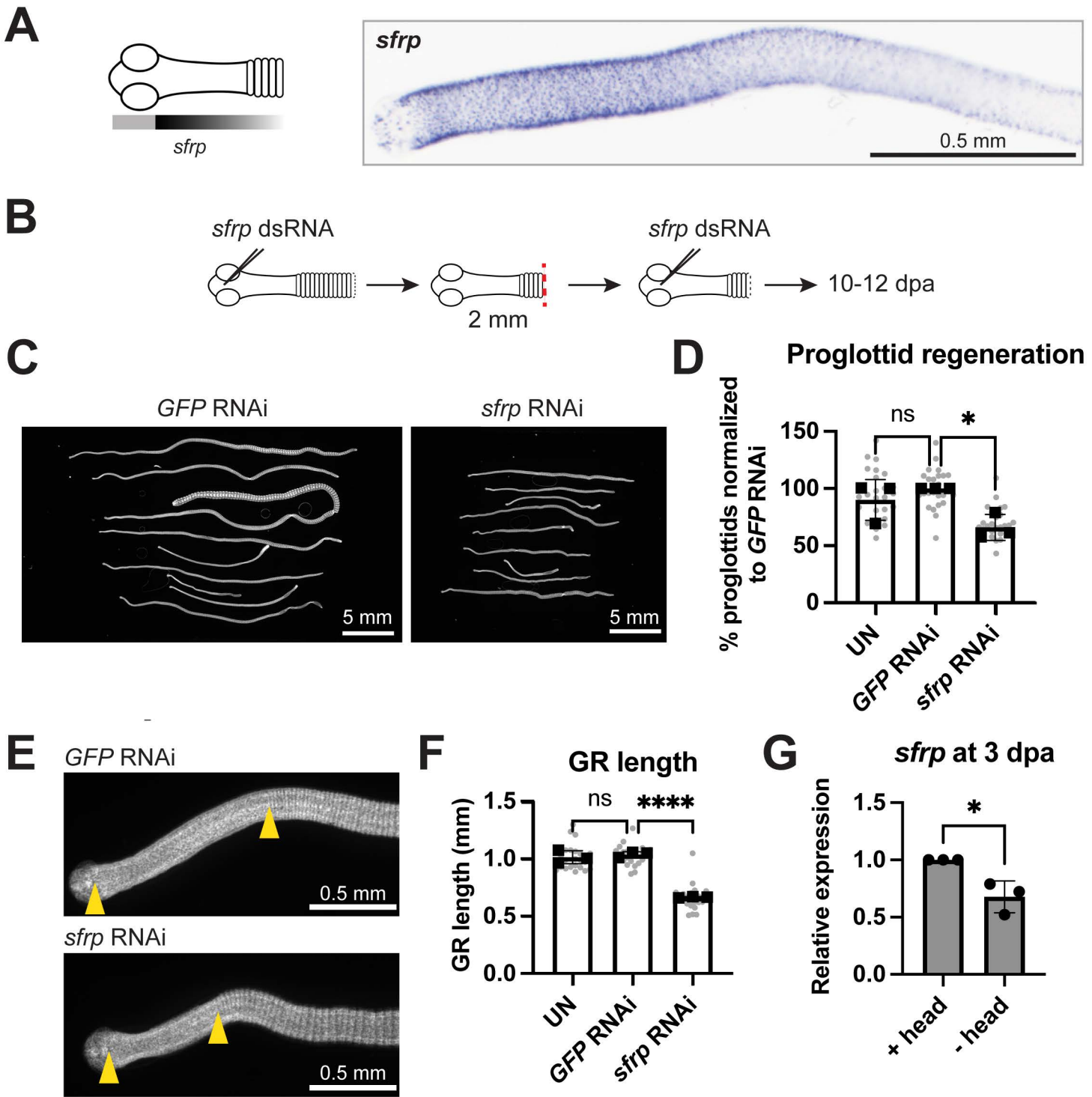
A
sfrp
sfrp
0.5 mm
B
sfrp dsRNA
sfrp dsRNA
2 mm
10-12 dpa
C
GFP RNAi
sfrp RNAi
5 mm
5 mm
D
Proglottid regeneration
% proglottids normalized to GFP RNAi
ns
*
150
100
50
0
UN
GFP RNAi
sfrp RNAi
E
GFP RNAi
0.5 mm
sfrp RNAi
0.5 mm
F
GR length
GR length (mm)
ns
****
1.5
1.0
0.5
0.0
UN
GFP RNAi
sfrp RNAi
G
sfrp at 3 dpa
Relative expression
*
1.5
1.0
0.5
0.0
+ head
- head

Figure 7

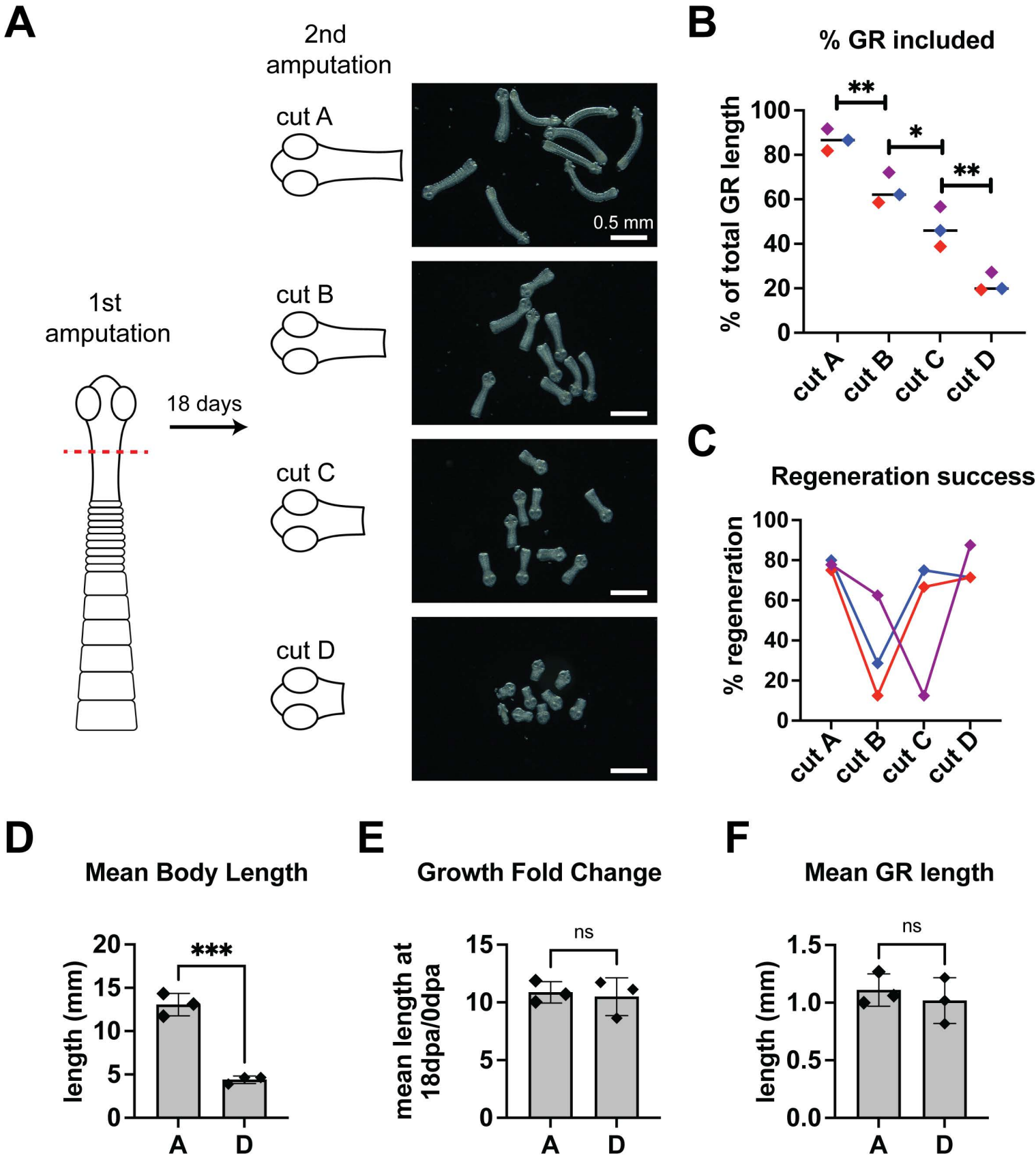
A
2nd amputation
cut A
cut B
cut C
cut D
0.5 mm
1st amputation
18 days
B
% GR included
% of total GR length
100
80
60
40
20
0
**
*
**
cut A
cut B
cut C
cut D
C
Regeneration success
% regeneration
100
80
60
40
20
0
cut A
cut B
cut C
cut D
D
Mean Body Length
length (mm)
20
15
10
5
0
***
A
D
E
Growth Fold Change
mean length at 18dpa/0dpa
15
10
5
0
ns
A
D
F
Mean GR length
length (mm)
1.5
1.0
0.5
0.0
ns
A
D

Figure 8

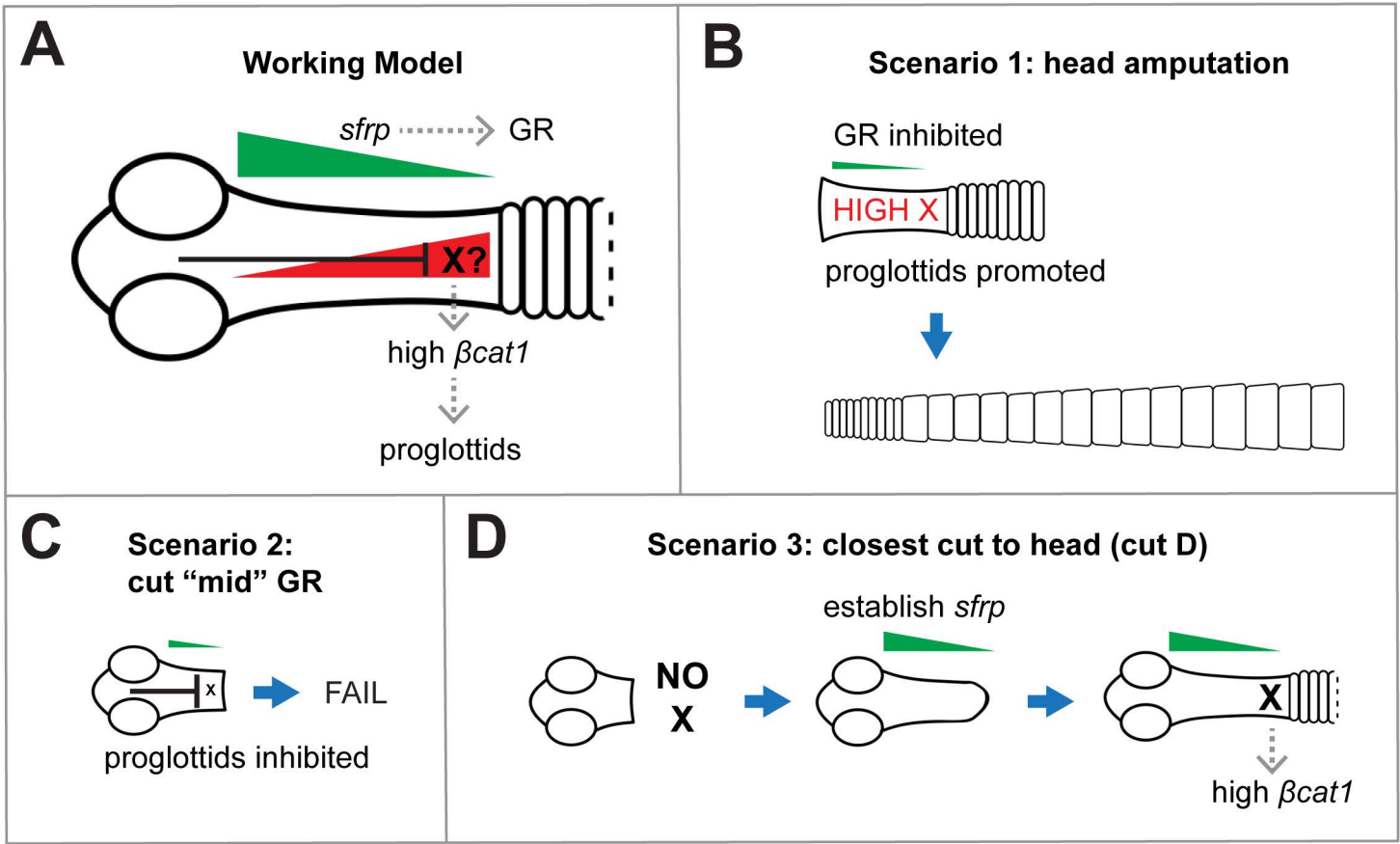
A
Working Model
sfrp
GR
X?
high βcat1
proglottids
B
Scenario 1: head amputation
GR inhibited
HIGH X
proglottids promoted
C
Scenario 2:
cut "mid" GR
X
FAIL
proglottids inhibited
D
Scenario 3: closest cut to head (cut D)
establish sfrp
NO
X
X
high βcat1

Figure S1

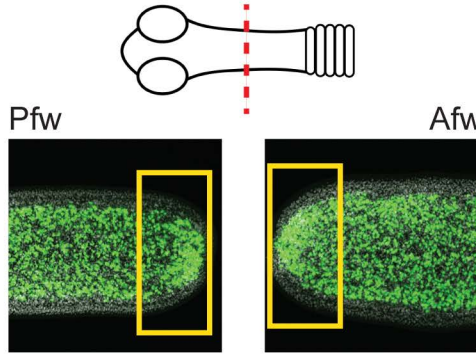
Pfw
Afw

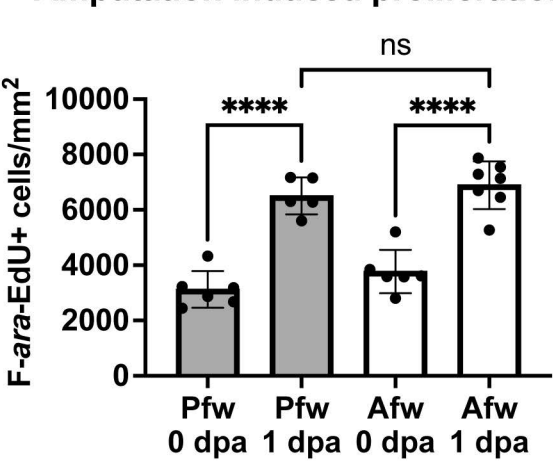
Amputation induced proliferation
ns
****
****
F-ara-EdU+ cells/mm2
10000
8000
6000
4000
2000
0
Pfw 0 dpa
Pfw 1 dpa
Afw 0 dpa
Afw 1 dpa

Figure S2

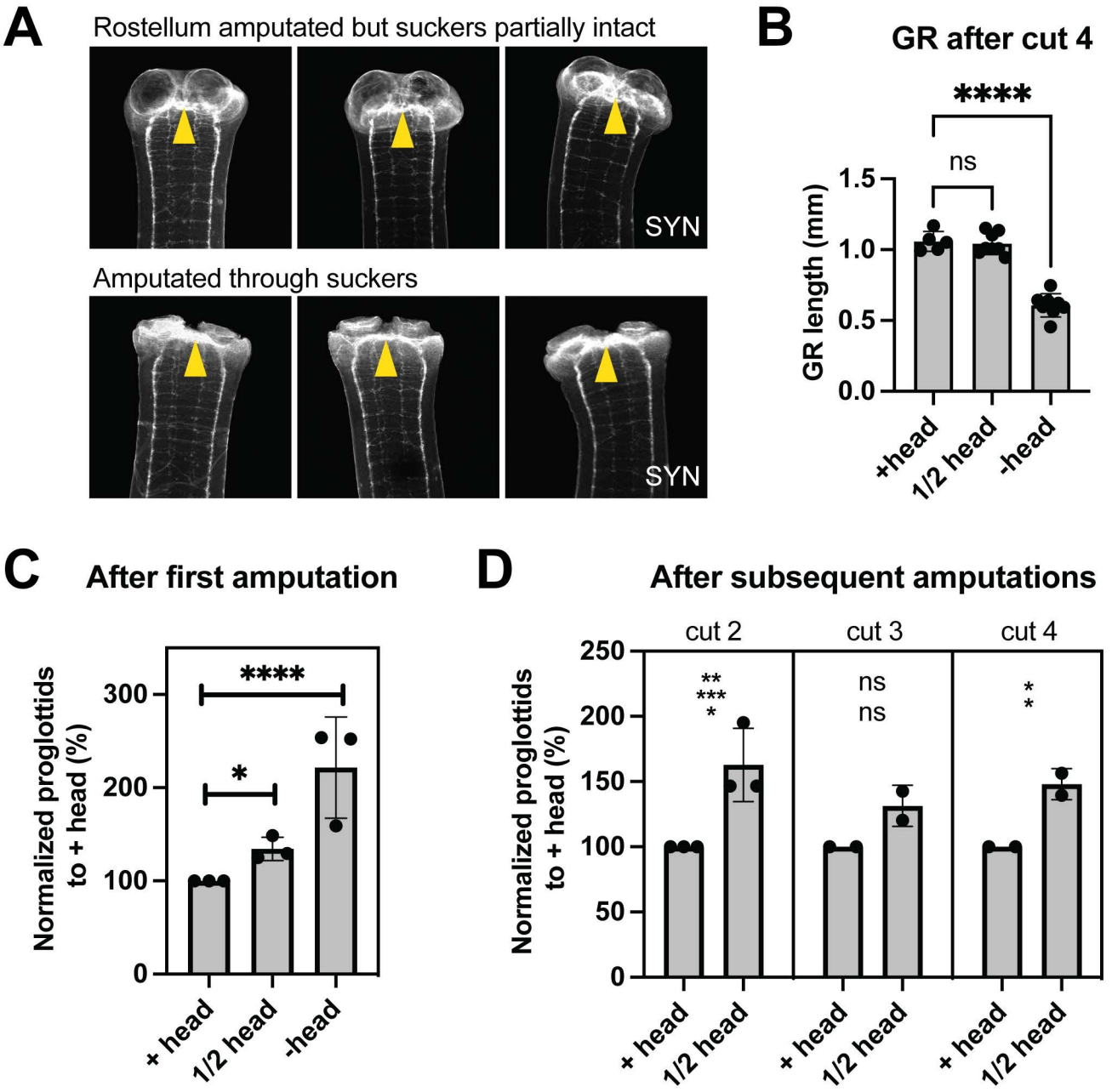
A
Rostellum amputated but suckers partially intact
SYN
Amputated through suckers
SYN
B
GR after cut 4
****
ns
GR length (mm)
1.5
1.0
0.5
0.0
+head
1/2 head
-head
C
After first amputation
****
*
Normalized proglottids to + head (%)
300
200
100
0
+ head
1/2 head
-head
D
After subsequent amputations
cut 2
cut 3
cut 4
**
***
*
ns
ns
*
*
Normalized proglottids to + head (%)
250
200
150
100
50
0
+ head
1/2 head
+ head
1/2 head
+ head
1/2 head

Figure S3

A

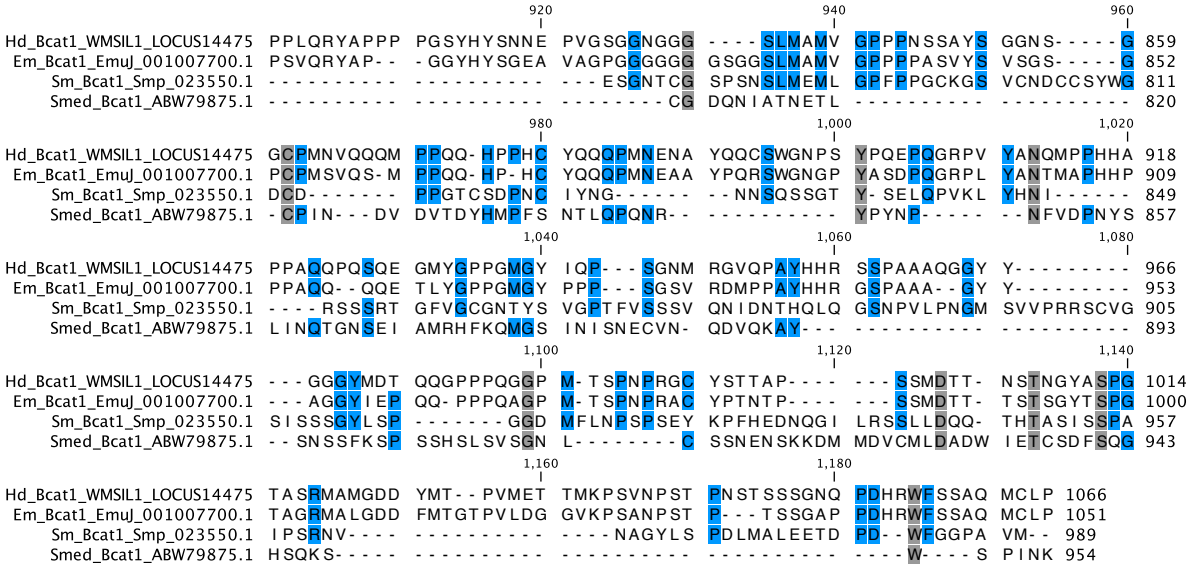

B

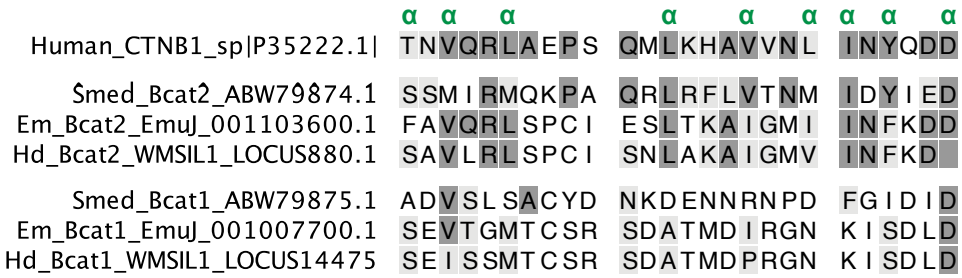

Figure S4

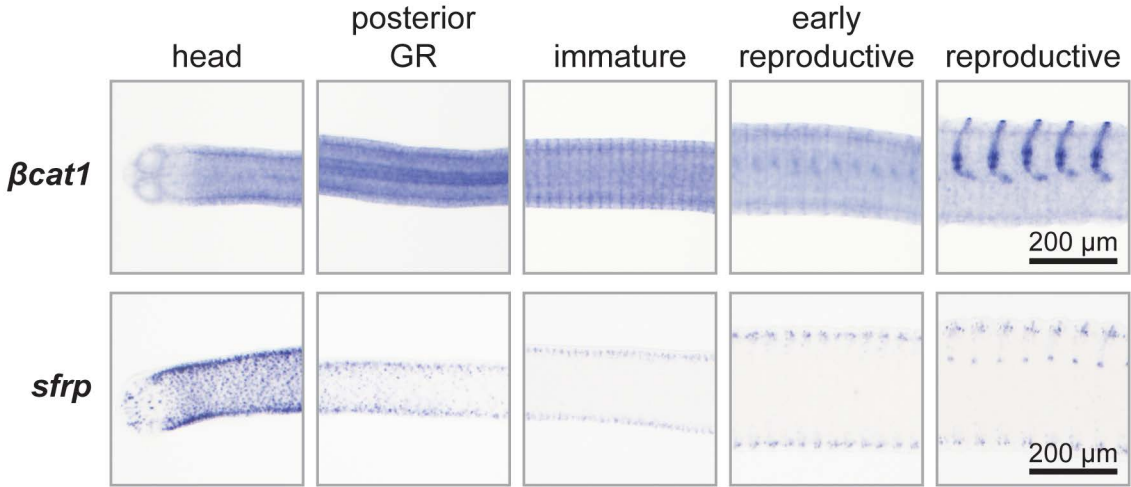
head
posterior GR
immature
early reproductive
reproductive
βcat1
sfrp
200 μm
200 μm

Figure 95

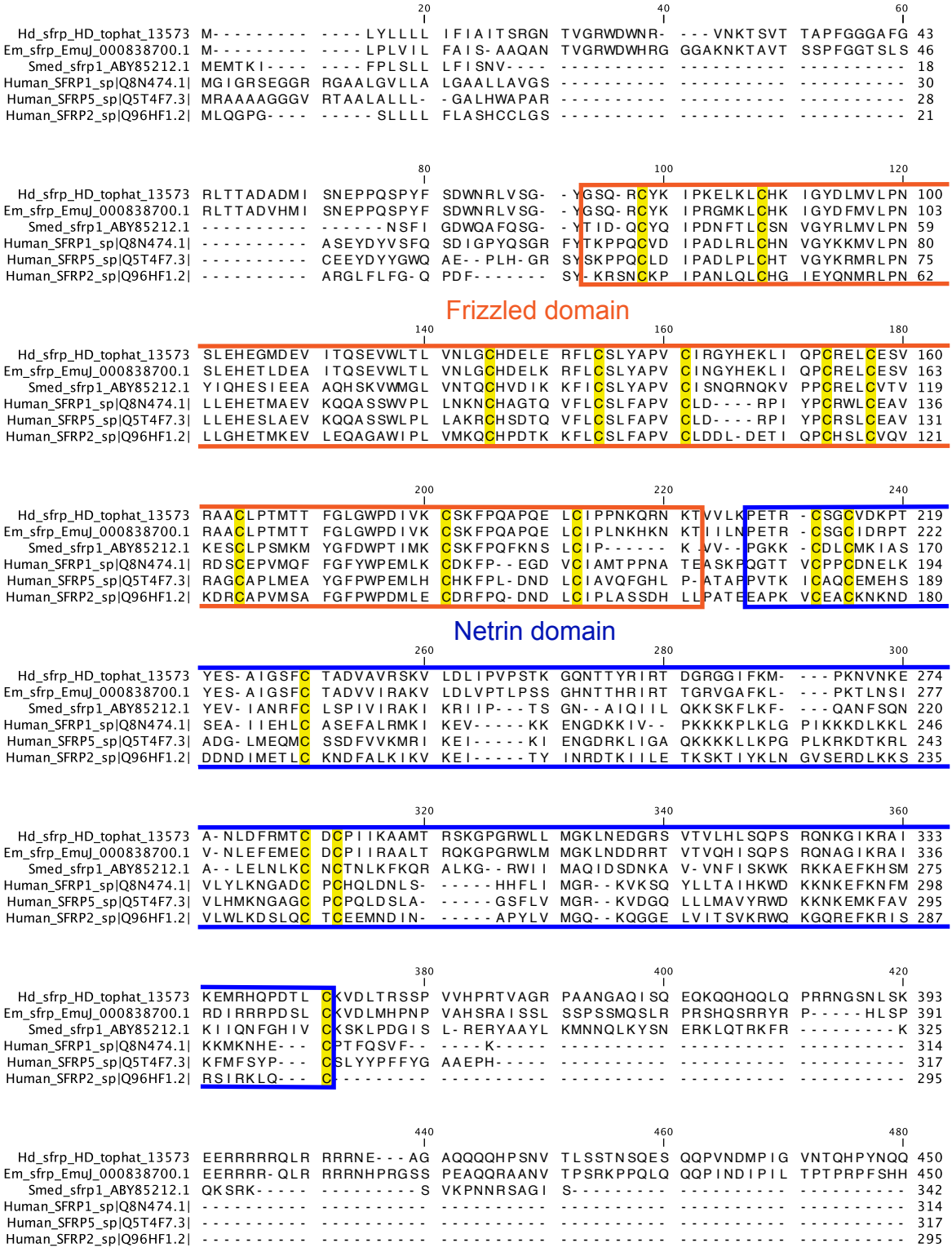

Figure S6

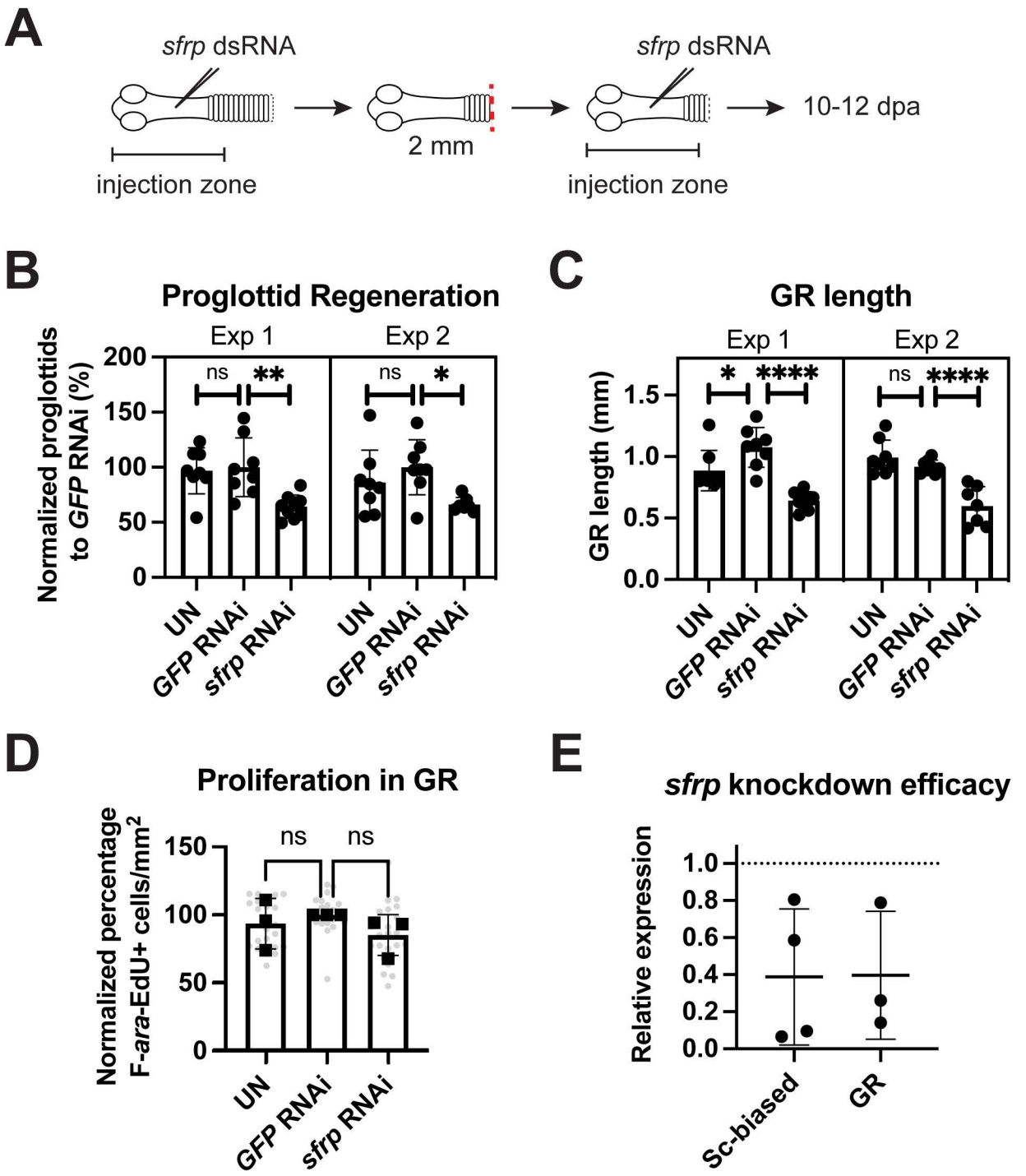
A
sfrp dsRNA
2 mm
sfrp dsRNA
10-12 dpa
injection zone
injection zone
B
Proglottid Regeneration
Exp 1
Exp 2
Normalized proglottids to GFP RNAi (%)
ns
**
ns
*
UN
GFP RNAi
sfrp RNAi
C
GR length
Exp 1
Exp 2
GR length (mm)
*
****
ns
****
D
Proliferation in GR
Normalized percentage F-ara-EdU+ cells/mm2
ns
ns
E
sfrp knockdown efficacy
Relative expression
Sc-biased
GR

Figure S7

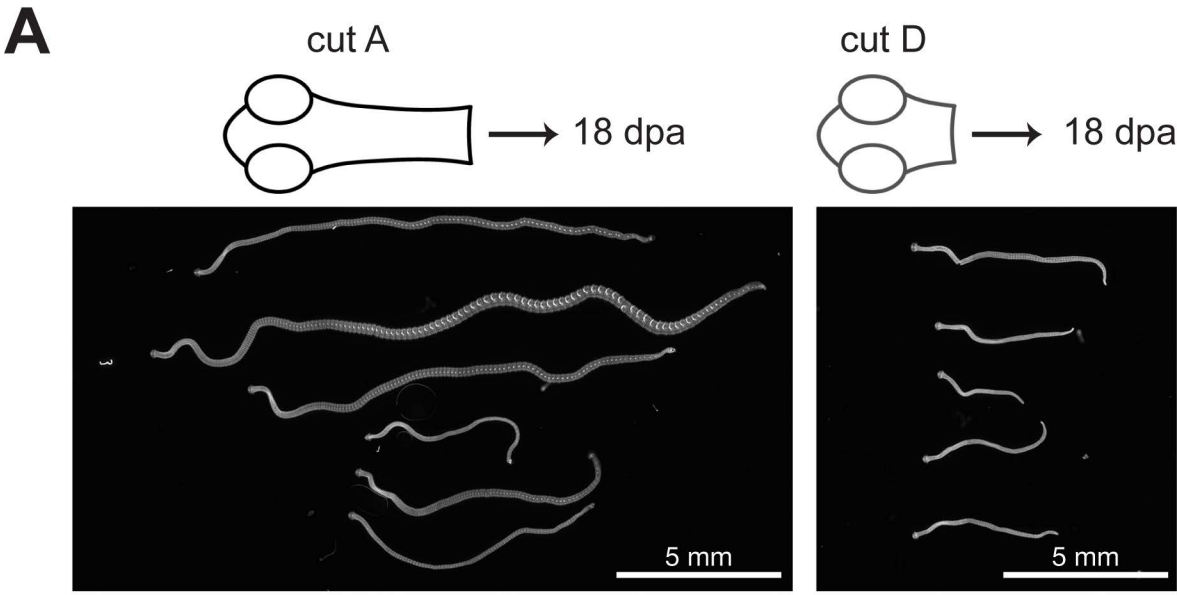
A
cut A
18 dpa
cut D
18 dpa
5 mm
5 mm

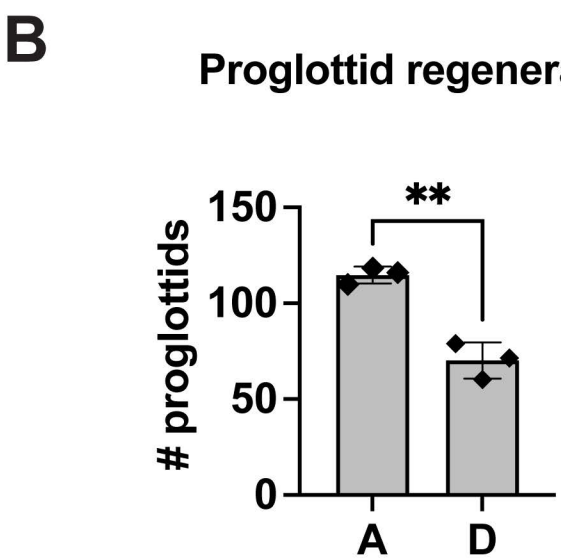
B
Proglottid regeneration
proglottids
150
100
50
0
**
A
D